# Zinc stimulation of phytoplankton in a low carbon dioxide, coastal Antarctic environment: evidence for the Zn hypothesis

Riss M. Kell[1,+], Adam V. Subhas[1], Nicole L. Schanke[2], Lauren E. Lees[3], Rebecca J. Chmiel[1], Deepa Rao[1], Margaret M. Brisbin[1], Dawn M. Moran[1], Matthew R. McIlvin[1], Francesco Bolinesi[4], Olga Mangoni[4], Raffaella Casotti[5], Cecilia Balestra[6], Tristan J. Horner[1], Robert B. Dunbar[7], Andrew E. Allen[8,9], Giacomo R. DiTullio[2], Mak A. Saito[1*]

[1]Department of Marine Chemistry and Geochemistry, Woods Hole Oceanographic Institution, Woods Hole, MA, 02543, USA

[2]Hollings Marine Laboratory, College of Charleston, Charleston, SC, 29424, USA

[3]Department of Ecology and Evolutionary Biology, University of California at Irvine, Irvine, CA, 92697, USA

[4]Department of Biology, Università degli Studi di Napoli Federico II, Complesso di Monte Sant'Angelo, Via Cinthia 21, 80126, Napoli, Italy

[5]Department of Integrative Marine Ecology, Stazione Zoologica Anton Dohrn, Villa Comunale, 80121, Naples, Italy

[6]National Institute of Oceanography and Applied Geophysics, 34010 Sgonico (TS), Italy

[7]Doerr School of Sustainability, Stanford University, Stanford, CA, 94305, USA

[8]Microbial & Environmental Genomics, J. Craig Venter Institute, San Diego, CA, 92093, USA

[9]Scripps Institution of Oceanography, Integrative Oceanography Division, University of California, San Diego, CA, 92037, USA

*Correspondence to:* Mak A. Saito (msaito@whoi.edu)

[+]Formerly published under Riss Kellogg; now affiliated with Gloucester Marine Genomics Institute, Gloucester MA, 01930

**Abstract.**

The ocean acts as a carbon sink, absorbing carbon from the atmosphere and resulting in substantial uptake of anthropogenic $CO_2$ emissions. As biological processes in the oceans such as net primary production (NPP) contribute significantly to this sink, understanding how they will shift in response to increasing atmospheric $CO_2$ is necessary to project future ocean carbon storage capacity. Macronutrient and micronutrient resource limitation within the oceans regulates NPP, and while some micronutrients such as zinc (Zn) are present at very low concentrations, their ability to limit NPP has remained unclear. Zn is a key micronutrient used by phytoplankton for a multitude of metabolic functions, yet there have been few observations of its influence on natural oceanic phytoplankton populations. In this study, we observed Zn limitation of growth in the natural phytoplankton community of Terra Nova Bay, Antarctica, in addition to primary iron (Fe) limitation. Shipboard incubation experiments amended with Zn and Fe resulted in significantly higher chlorophyll *a* content and dissolved inorganic carbon drawdown compared to Fe addition alone. Zn and Fe stress response proteins detected in incubation and environmental biomass provided independent verification of algal co-stress for these micronutrients. We consider total biomass and low surface ocean $pCO_2$ as potential drivers of environmental Zn stress. This study definitively establishes that Zn limitation can occur in the modern oceans, opening up new possibility space in our understanding of nutrient regulation of NPP through geologic time, and we consider the future of oceanic Zn limitation in the face of climate change.

## 1 Introduction

Primary productivity in the oceans is a key component of the global carbon cycle and is largely controlled by the availability of nitrogen (N), phosphorus (P), and iron (Fe). Yet there is increasing evidence that other micronutrients such as zinc (Zn), cobalt (Co), and vitamin $B_{12}$ can also influence phytoplankton productivity, often as secondary limiting nutrients after N, P, or Fe are added (Moore et al. 2013). Zn can be particularly scarce in the photic zone (Bruland 1980; Jakuba et al. 2012) where total dissolved Zn ($dZn_T$) can be below 0.2 nM in seawater due to biological uptake and complexation by organic ligands (Bruland 1989; Lohan et al. 2002; Baars and Croot 2011; Middag et al. 2019), which further lowers Zn bioavailability (Sunda and Huntsman 2000; Saito et al. 2008; Lhospice et al. 2017). Marine eukaryotic algae and copiotrophic bacteria possess a large metabolic demand for Zn that is on par with that of Fe (Sunda and Huntsman 2000; Mazzotta et al. 2021) and polar phytoplankton in particular demonstrate an enhanced Zn demand based on genomic and laboratory analyses (Ye et al. 2022). Despite the scarcity of bioavailable Zn in the surface ocean and its high cellular demand, relatively few experimental studies have examined the ability of Zn addition to stimulate natural phytoplankton communities **(Supplementary Table 1)**. These results have been variable with findings that include negative results (Scharek et al. 1997; Coale et al. 2003; Ellwood 2004), slight Zn stimulatory results (Crawford et al. 2003), a “very small increase” relative to controls in an unreplicated experiment (Coale et al. 2003), Zn stimulation within Fe and Si uptake experiments (Franck et al. 2003), Zn primary and secondary limitation in the North Pacific in an unreplicated experiment (Jakuba et al. 2012), secondary Zn limitation after primary Si limitation in the Costa Rica Dome (Dreux Chappell et al. 2016), and enhanced Zn uptake rates under low $pCO_2$ (Xu et al. 2012). Whether due to the early negative results, the few positive findings, or a general prejudice against considering additional factors in controlling marine productivity, it is

our experience that there is currently no broad community recognition that zinc limitation is a process that could affect primary productivity in any region of the oceans, leaving the original 'zinc hypothesis' unresolved (Morel et al. 1994).

In juxtaposition, laboratory studies have unequivocally demonstrated that marine phytoplankton can easily be Zn-limited in culture, and that Zn stress is exacerbated by low $CO_2$ due to an inability to synthesize the metalloenzyme carbonic anhydrase and resultant carbon co-limitation (Morel et al. 1994; Buitenhuis et al. 2003; Sunda and Huntsman 2005). In this study, we reconcile these perspectives with a comprehensive, multipronged study of the natural phytoplankton assemblage in Terra Nova Bay (TNB), Antarctica, documenting evidence of Fe and Zn stress in a low $pCO_2$ coastal environment.

## 2 Results

### 2.1 Biogeochemical characterization of Terra Nova Bay

Terra Nova Bay (TNB), Antarctica, was temporally sampled for over one month (January 9 – February 18, 2018) during the 2017-2018 CICLOPS expedition **(Fig. 1a; Supplementary Table 2)** to concurrently characterize the natural progression of the phytoplankton bloom and biogeochemical changes in the water column (Kell et al. 2024). Surface waters within TNB had low (~200 μatm) seawater $pCO_2$ (**Fig. 1b**) which contrasted with measurements >400 μatm further from the study site (**Fig. 1c**). A large phytoplankton bloom was present as indicated by high (> 3000 ng $L^{-1}$) chlorophyll fluorescence concentrations in January that waned into February (**Fig. 1d**), characteristic of Antarctic polynya environments. This phytoplankton community initially consisted of a mixed assemblage of both diatoms as indicated by fucoxanthin (fuco, **Fig. 1e**) and *Phaeocystis* as verified by shipboard microscopy and as indicated by 19'-hexanoyloxyfucoxanthin (19'-hex, **Fig. 1f**). Surface fucoxanthin concentrations

>200 ng $L^{-1}$ were observed at the late TNB stations (**Fig. 1e**) while 19'-hex decreased to ~20 ng $L^{-1}$ (**Fig. 1f**), indicating that the stations sampled in late February were dominated by diatoms rather than *Phaeocystis*. This was consistent with historical observations of phytoplankton succession patterns in TNB (DiTullio and Smith 1996; Smith et al. 2006; Mangoni et al. 2019). Pronounced and progressively deepening total dissolved Zn ($dZn_T$) depletion over time was observed, with dZn depleted down to an average of 0.82 ± 0.47 nM at 10 m over all TNB stations (**Fig. 1g**). The Zn-depleted area of the water column progressively deepened to 50 m and then to ~100 m throughout January and February **(Fig. 1g),** indicative of strong Zn uptake and export from the euphotic zone. Total Zn uptake ($\rho$Zn, measured concurrently using a stable isotope tracer method) (Kell et al. 2024) was highest in the shallow euphotic zone in early January and waned into February (**Fig. 1h**), following trends seen in chlorophyll fluorescence (**Fig. 1d**) and 19'-hex (**Fig. 1f**). This $\rho$Zn trend was consistent with laboratory studies demonstrating the substantial Zn requirements of both diatoms and *Phaeocystis antarctica* (Saito and Goepfert 2008; Kellogg et al. 2020). Across all TNB stations, total dissolved Fe ($dFe_T$) in the upper 50 m remained below 1 nM (**Fig. 1i**) as observed previously in this region (Fitzwater et al. 2000). In the Ross Sea, dissolved iron (dFe) has previously been demonstrated to be the primary limiting nutrient for phytoplankton growth (Martin et al. 1990; Coale et al. 2003; Sedwick et al. 2011).

### 2.2 Biogeochemical characterization of the incubation study site

Within TNB station, station 27 (referred to as the "experimental site" herein) was chosen for the multifactor shipboard incubation experiment (**Fig. 1a,b**; red star). This site harbored a coastal bloom and was biologically and chemically characterized as having high *in situ*

chlorophyll *a* levels (maximum of 3259 ng $L^{-1}$ at 30 m; **Fig. 1j**) and was comprised of diatoms as indicated by fucoxanthin and *Phaeocystis* as indicated by 19'-hex (**Fig. 1k**). A decrease in surface total dissolved inorganic carbon ($DIC_T$; 2181 μmol $kg^{-1}$ at 15 m compared to the deep water (200-1065 m) average of 2224 ± 2.1 μmol $kg^{-1}$**, Fig. 1l**) was also observed. Within the water column, dZn demonstrated a pronounced decrease from 5.1 nM at 50 m to 0.9 nM at 10 m, representing an 82% decrease (and a 76% decrease comparing the minimum $dZn_T$ value at 10 m to the average deepwater (210 – 1000 m) concentration of 3.9 nM ± 0.4; **Fig. 1m**), consistent with prior observations of surface dZn depletion in this region (Fitzwater et al. 2000).

Observations of rapid Zn uptake (46 pmol $L^{-1}$ $d^{-1}$ at 10 m) at the experimental site (**Fig. 1n**) likely contributed to this surface depletion, as Zn uptake rates of this magnitude are of the appropriate scale to induce the multi-nanomolar surface water depletion during the austral spring and summer season (Kell et al. 2024). Consistent with high macronutrient abundance in this region, surface macronutrient concentrations (nitrate and nitrite, phosphate, and silicic acid) were partially depleted at the experimental site with 64%, 46%, and 29% decreases in N+N, P, and Si, respectively, comparing 10 m and average deep water (200 – 1000 m) values (**Fig. 1o**).

### 2.3 Evidence for Zn stimulation of phytoplankton: experimental site shipboard incubations

A multifactor incubation experiment was conducted using surface waters collected at the experimental site by trace metal clean fish sampler (7 m) fed into a shipboard cleanroom to examine controls on net primary productivity, with triplicate treatments of Zn amended (+Zn; 2 nM as $ZnCl_2$), Fe amended (+Fe; 1 nM as $FeCl_2$), and Fe and Zn amended (+Fe+Zn) incubations, in addition to unamended controls. Addition of Fe alone (+Fe) resulted in significantly higher chl *a* content compared to controls ($p$ = 9.5e-5) after six days (T6) (**Fig. 2a**), demonstrating primary

Fe limitation as observed previously in the Ross Sea (Martin et al. 1990; Mangoni et al. 2019). However, addition of Zn alone (+Zn) also resulted in significantly higher chl *a* content compared to the controls ($p$ = 0.011), implying that a subset of the incubated phytoplankton population benefitted from the addition of Zn alone, without additional Fe, and may thus have been experiencing primary Zn limitation (**Fig. 2a**). The combined addition of +Fe+Zn resulted in the highest average chl *a* content among all treatments at T6, with 4.5 ± 0.21 μg $L^{-1}$ compared to 3.9 ± 0.35 μg $L^{-1}$ and 2.8 ± 0.15 μg $L^{-1}$ achieved by +Fe and +Zn alone, respectively, demonstrating additive co-limitation between Zn and Fe (Sperfeld et al. 2016). The Zn stock solution was analyzed to confirm these results were not caused by inadvertent iron contamination (see Methods). Significant differences in seawater chemistry were also observed within these incubations over time, with larger decreases in $DIC_T$ in all metal treatments compared to the control (-12.7 μmol $kg^{-1}$ for +Fe ($p$ = 5.3e-6), -8.2 μmol $kg^{-1}$for +Zn ($p$ = 5e-5), and -18.5 μmol $kg^{-1}$ for +Fe+Zn ($p$ = 2.2e-16); **Fig. 2b**). The decrease in $DIC_T$ observed with +Fe+Zn was significantly larger than that achieved with +Fe alone ($p$ = 4.4e-3; **Fig. 2b**). Statistically significant differences in measured parameters among treatments are summarized in **Supplementary Table 3.**

Further consistent with the observed Zn stimulation of biomass in the incubations, the largest decreases in macronutrient (P and N+N) concentrations in these incubations at T6 were observed in the +Fe+Zn treatment (**Supplementary Figure 1a,b**), as was the largest increase in particulate organic carbon (POC; **Supplementary Figure 1c**). POC collected from the +Zn and +Fe+Zn incubations was characterized by larger C:N atomic ratios (5.9 and 6.2, respectively) compared to the +Fe and T6 control (5.2 and 5.3; **Supplementary Figure 1d**). Significantly higher bacterial abundances in both +Fe ($p$ = 9.1e-4) and +Fe+Zn ($p$ = 6.3e-4) treatments relative

to the T6 control (**Supplementary Figure 1e**) indicated the alleviation of bacterial Fe limitation, consistent with prior reports (Obernosterer et al. 2015; Fourquez et al. 2020; Sun et al. 2021).

At the conclusion of the incubation experiments, biomass was collected via filtration and proteomic analysis was performed (see Methods) and analyzed for biomarkers of Zn and Fe stress. We detected both algal Fe- and Zn-stress proteins, which provided an independent line of evidence corroborating the results described above (**Fig. 2c**). This included the detection of the Zn/Co responsive protein ZCRP-A (a putative Zn chaperone) (Kellogg et al. 2022a) as a biomarker of Zn stress as well as the iron starvation-induced proteins ISIP1A, ISIP2A and ISIP3 (ISIPs) as biomarkers of Fe stress (**Supplementary Table 4**). The ISIPs represent a group of unrelated proteins that are upregulated under Fe limitation in various algal species. ISIP1 proteins are responsible for endocytosis of siderophore-bound iron, ISIP2 proteins are involved in $Fe^{3+}$ uptake, and ISIP3 has been suggested to act as an Fe storage protein (Allen et al. 2008; Behnke and LaRoche 2020). RUBISCO abundance within each treatment is shown in **Fig. 2c** as a proxy for the potential phytoplankton production. Within the T6 incubation biomass, there was an increased abundance of ISIPs in the control and +Zn treatment, and a decrease in ISIP protein abundance within the +Fe and +Fe+Zn treatments, consistent with primary Fe limitation and the expected response to Fe addition (**Fig. 2c**). ISIPs were taxonomically assigned to diatoms, *Phaeocystis*, and dinoflagellates (**Fig. 2d**). The strongest expression of ZCRP-A protein was detected in the +Fe treatment (**Fig. 2c,d**) indicative of Fe addition driving the community towards increased Zn stress. Notably, ZCRP-A was still detected in the +Fe+Zn treatment (**Fig. 2c,d**), implying that the added Zn was unable to completely satiate Zn demand as phytoplankton biomass increased (as indicated by the increase in chl *a* at T6, **Fig. 2a**), despite added Zn (2 nM) being double that of added Fe (1 nM). Sequence analysis of the contigs identified as ZCRP-A

homologs in these incubations revealed that all contigs contained one or more canonical conserved motifs found in COG0523 family proteins such as ZCRP-A (**Supplementary Figure 2)**. Coupled with evidence from prior laboratory studies (Kellogg et al. 2022a), this provides further support for the role of ZCRP-A in responding to Zn scarcity. ZCRP-A proteins were taxonomically assigned to chlorophytes, dinoflagellates, and *Phaeocystis*, with the detection of *Phaeocystis* ZCRP-A only in the +Fe treatment (**Fig. 2d**). The detection of ZCRP-A attributed to *Phaeocystis*, but the nondetection of ZCRP-A attributed to diatoms, implies that diatoms present in these incubations (as indicated by diatom RUBISCO; **Fig. 2d**) were outcompeting *Phaeocystis* for Zn. Our observations of Fe and Zn biomarkers shifting in abundance in response to their respective metal treatment provides independent evidence for Zn/Fe co-limitation.

**2.4 Taxonomic characterization of incubation results**

To characterize the phytoplankton species responding to metal amendment, we measured phytoplankton pigments within the shipboard incubations over time, which revealed a diverse taxonomic response to metal amendments. Measured pigments included fucoxanthin (fuco), 19'-hexanoyloxyfucoxanthin (19'-hex), prasinoxanthin (prasino), chlorophyll *b* (chl *b*), and chlorophyll c3 (chl c3). Fuco is produced by both diatoms and by *Phaeocystis* under certain conditions, while 19'-hex and chl c3 are indicative of *Phaeocystis* in the Southern Ocean (DiTullio et al. 2007). Fuco:19'-hex ratios significantly increased in the +Fe ($p$ = 4.2e-4) and +Fe+Zn treatments ($p$ = 2.7e-3) (**Supplementary Figure 3a**) due to no significant change in fuco (**Supplementary Figure 3b**) and decreased 19'-hex (**Supplementary Figure 3c**) relative to the T6 control. *Phaeocystis* contributions to total fuco concentrations are typically minimal at the low Fe levels of the Ross Sea, though *Phaeocystis* can revert to making fuco rather than 19'-hex

when released from Fe limitation (DiTullio et al. 2007), as was evident in these incubations by decreased 19'-hex:chl c3 ratios within the +Fe and +Fe+Zn treatments (**Supplementary Figure 3d**). *Phaeocystis* therefore likely contributed to total fuco by responding to Fe addition. Notably, significant decreases in both fuco:chl *a* and 19'-hex:chl *a* (**Supplementary Figure 3e,f**) in all treatments compared to the T6 control indicated that other phytoplankton groups contributed to chl *a* (**Fig. 2a**) without contributing fuco nor 19'hex. Increases in chl *b* (**Supplementary Figure 3g**) and prasinoxanthin (**Supplementary Figure 3h**) suggest that small green algae such as chlorophytes and prasinophytes also responded to +Fe and +Zn independently, consistent with the detection of chlorophyte ZCRP-A in these incubations **(Fig. 2d**). Photosynthetic efficiency of photosystem II (Fv/Fm) significantly increased with +Fe ($p = 0.011$) and with +Fe+Zn ($p = 0.0036$) at T4 (day 4) compared to T4 controls, but did not significantly increase with +Zn alone, implying Fv/Fm may not be useful as a diagnostic for Zn stress and that caution should be used in interpreting its signals universally (**Supplementary Figure 3i**). No significant difference in Fv/Fm was observed among treatments at T6. Selective zooplankton grazing on small diatoms and solitary *Phaeocystis* cells may have played a role in affecting phytoplankton biomass and the observed pigment:chl *a* ratios. For instance, higher ratios of phaeophytin:total phaeopigments were observed in +Fe and +Zn amended incubations (**Supplementary Figure 4**) which may reflect grazing on solitary *Phaeocystis* cells, as high phaeophytin:total phaeopigments ratios were previously observed in *Phaeocystis* dominated waters of the Ross Sea (DiTullio and Smith 1996).

**2.5 Detection of Zn- and Fe-stress protein biomarkers in the water column**

Metaproteomic and metatranscriptomic analyses of biomass within the water column at the experimental site provided additional confirmation of the incubation results, as we detected

Zn- and Fe- stress-response proteins present within the water column, which were therefore naturally present without influence from incubation conditions. In addition to ISIPs and ZCRP-A, we detected ZCRP-B (a putative membrane-tethered Zn-binding protein) (Kellogg et al. 2022a), Zrt/Irt-like (ZIP) Zn transporters (which are known to be used by marine phytoplankton for uptake of $Zn^{2+}$ and other divalent metal cations (Allen et al. 2008; Milner et al. 2013; Bender et al. 2018)), and θ (theta) and δ (delta) carbonic anhydrases (CAs). θ-CAs with $Zn^{2+}$ coordination sites have been documented in diatoms (Jensen et al. 2020), including the polar diatom *Chaetoceros neogracile* RS19 (Kellogg et al. 2022b), but no studies to date have investigated enzyme activity nor efficiency with $Co^{2+}$ or $Cd^{2+}$. In contrast, δ-CA (i.e, *Thalassiosira weissflogii* TWCA1) is known to function with either $Co^{2+}$ or $Zn^{2+}$ as a cofactor (Lane and Morel 2000b) conferring metabolic flexibility when $Zn^{2+}$ is scarce.

Both proteins and transcripts of Zn and Fe stress biomarkers (ZCRP-A and ISIPs) were observed throughout the water column at the experimental site. RUBISCO, ZCRP-A, and ISIP protein spectral counts were most abundant at the surface and decreased with depth within the within the 3μm size fraction (**Fig. 3a-c**), consistent with the depletion of trace metals in the photic zone due to high-biomass bloom conditions. ZCRP-A was detected in both 3 and 51 μm filter pore-size fractions (**Fig. 3b**) and was predominantly attributed to *Phaeocystis* and the diatom genus *Chaetoceros* in the euphotic zone, and predominantly to *Phaeocystis* and the diatom genus *Pseudo-nitzschia* in the mesopelagic zone (**Fig. 3i, Supplementary Figure 5a**). The presence of *Phaeocystis* below the photic zone is consistent with prior observations of rapid export of *Phaeocystis* cells (DiTullio et al. 2000). Throughout the water column, ISIPs were predominantly attributed to *Phaeocystis* and to the diatom genera *Fragilariopsis, Chaetoceros,* and *Pseudo-nitzschia* (**Fig. 3i, Supplementary Figure 5b**). We note that ZCRP-B, a protein also

found to be upregulated in marine diatoms under low Zn/Co and characterized as a putative membrane-tethered Zn/Co protein ligand (Kellogg et al. 2022a) was most abundant in the 0.2 μm fraction throughout the water column (**Fig. 3d**). As ZCRP-B shares ~30% similarity to the bacterial ABC-type nickel transporter component NikA, spectral counts within the bacterial 0.2 μm fraction most likely reflect true bacterial NikA. BLAST analysis of all ZCRP-B contigs confirmed that all ZCRP-B hits across all size fractions corresponded to bacteria (**Fig. 3i**).

ZIPs were almost solely detected in the 51 μm fraction, likely due to the capture of abundant *Phaeocystis* colonies and chain-forming diatoms (**Fig. 3e; Supplementary Figure 5c**). The assignment of the majority of ZCRP-A and ISIP proteins to *Phaeocystis* in the upper water column provides additional evidence that *Phaeocystis* was likely Zn/Fe co-limited at the study site, consistent with incubation results (**Fig. 2d**). The increased abundance of diatom θ-CA and δ-CA proteins within the water column (**Fig. 3f,g**), as well as transcripts for the diatom Cd carbonic anhydrase CDCA, which can replace $Zn^{2+}$ with $Cd^{2+}$ as the catalytic cofactor (Lane and Morel 2000a), in the 3 μm and 51 μm fractions at 200 m (**Fig. 3h**) was indicative of a sinking, prior diatom bloom event (Subhas et al. 2019). θ-CA and δ-CA were predominantly taxonomically assigned to the diatom genera *Chaetoceros* and *Pseudo-nitzschia*, respectively, while CDCA transcripts belonged to the diatom genera *Chaetoceros* and *Corethron* (**Fig. 3i**). The presence of θ-CA, but lack of δ-CA, assigned to *Chaetoceros* is consistent with proteomic analysis of the polar diatom *Chaetoceros neogracile* RS19 grown in culture under Zn limiting conditions (Kellogg et al. 2022b).

### 2.6 Zn:P ratios of the surface seawater at the experimental site

A third independent line of evidence for the nutritional influence of Zn scarcity on TNB phytoplankton was obtained from *in situ* cellular stoichiometry. Particulate Zn:P ratios (Zn:P) analyzed from biomass collected at the surface of this experimental station were consistent with ratios from Zn-limited culture studies. Particulate Zn:C ratios reported previously in Zn-limiting culture studies of the diatom *Thalassiosira pseudonana* (Sunda and Huntsman 2005) were converted to Zn:P ratios using the Redfield ratio (Redfield 1958) (**Supplementary Table 5**). We then compared these ratios and associated growth rates with particulate Zn:P measured within biomass collected at 10, 25, 50 and 100 m at the experimental site. At each of these surface depths, Zn:P measured at the experimental site was ~ 2E-4 mol:mol, which, in comparison to cultured diatom Zn:P ratios, fell within the range of severely Zn-limited growth rates (**Supplementary Figure 6**), again demonstrating the propensity for Zn-limited growth in this region and corroborating the incubation results.

## 3 Discussion

Antarctic waters are generally considered to not be prone to Zn limitation, given that high (> 1nM) dZn concentrations are typically observed in surface Southern Ocean waters (Coale et al. 2003). However, we observed multiple independent lines of evidence from both the field incubation experiment (chlorophyll, DIC, Zn and Fe biomarker proteins) and contextual environmental biogeochemical data of the water column at the incubation site (dZn, Zn uptake rates, pigments, cellular Zn:P stoichiometry, metaproteomic, and metatranscriptomic analyses) demonstrating that phytoplankton within Terra Nova Bay of the Ross Sea, Antarctica, were experiencing Zn and Fe nutritional stress.

Multiple factors could be considered as potential drivers in the creation of Zn-limiting conditions in the field, including Zn demand imposed by total biomass and the species comprising this biomass. The phytoplankton bloom observed during this expedition was comprised primarily of diatoms and *Phaeocystis*, consistent with previous Ross Sea seasonal blooms (Smith et al. 2006; Arrigo et al. 2012; Mangoni et al. 2019), and which contributed to the observed high Zn uptake rates and thus surface Zn depletion (Kell et al. 2024), resulting in nutrient-like dZn profiles throughout TNB.

Our field observation of Zn limitation was made in an environment characterized by diminished $pCO_2$, which we consider as a factor potentially driving Zn stress. We observed a substantial drawdown of surface seawater $pCO_2$ to 221 μatm at the incubation site (a ~45% decrease compared to offshore waters in the Ross Sea measured during the same time frame; **Fig. 1b**). Laboratory studies have unequivocally demonstrated that marine phytoplankton can easily be Zn-limited in culture due to their large Zn requirement, and that this effect is exacerbated at low $pCO_2$ (Morel et al. 1994; Sunda and Huntsman 2005) due to the use of Zn as a required catalytic cofactor within carbonic anhydrase (CA) metalloenzymes (Sunda and Huntsman 2005). CAs catalyze the reversible dehydration of $HCO_3^-$ to $CO_2$, the substrate required by the carbon fixing enzyme RUBISCO. As $HCO_3^-$ constitutes about 90% of the dissolved inorganic carbon (DIC) pool in the surface ocean, sufficient CA activity prevents carbon stress in marine phytoplankton by ensuring adequate $CO_2$ supply to RUBISCO. It has therefore been hypothesized that the combination of high biomass and resulting low $CO_2$ may cause severe Zn depletion that may limit algal growth rates due to lack of Zn and thus reduced CA activity, and thus reduced availability of carbon for photosynthesis (Morel et al. 1994; Sunda and Huntsman 2005). This Zn-C limitation relationship is referred to as ‘biochemically dependent co-

limitation', in which the availability of one nutrient is essential for the acquisition or utilization of another nutrient, especially at low concentrations (Saito et al. 2008).

To explore this in the context of our field observations, using the available quantitative constraints on Zn and $CO_2$ co-limitation thresholds available from the literature (see Methods), we estimated that the threshold for Zn-$CO_2$ limitation in culture synthesized across many alga occurs at 259 μatm $pCO_2$. We then compared this laboratory-determined Zn/C limitation threshold estimate to both the *in situ* 221 μatm $pCO_2$ measured at our field study site, and to the historical, global trend in surface ocean $pCO_2$ (**Fig. 4a,b**). Global surface ocean $pCO_2$ levels are rapidly rising above both the laboratory-estimated 259 μatm $pCO_2$ Zn/C limitation threshold and our field observation value of 221 μatm (Jiang et al. 2023) (**Fig. 4a,b)**. Though only a fraction of the modern-day surface ocean is currently at ≤ 250 ppm $pCO_2$ (predominantly comprised of polar regions; **Fig. 4c**), this represents a large decrease in oceanic extent compared to only 100 years ago (**Fig. 4d**). Even though this may move the majority of oceanic regions farther from Zn and C limitation thresholds, there continue to be highly productive and episodic coastal blooming events that induce significant $pCO_2$ drawdown (Harrison et al. 2018; Dai et al. 2022). These coastal regions are increasingly recognized as being disproportionally significant contributors to global ocean carbon export (with respect to their area), particularly at the high latitudes (Harrison et al. 2018; Dai et al. 2022), and will hence continue to be prone to Zn stress at low $CO_2$ as we have observed. Many other coastal regions have been observed to experience depressed $CO_2$ such as the Amundsen Sea (Tortell et al. 2012), Amazon River plume (Valerio et al. 2021), the west Florida Shelf (Robbins et al. 2018), the East China Sea (Shim et al. 2007), the Northern Gotland Sea (Schneider and Müller 2018), and Monterey Bay, California (Chavez et al. 2018) to name a few examples.

## 4 Conclusions

Given the great challenge of conducting Zn manipulation experiments without contamination, we did not try to manipulate $pCO_2$ as an additional experimental treatment. Instead, we actively sought out a low $pCO_2$ environment for the study site, building on prior laboratory studies and a cadmium (Cd) $pCO_2$ field study (Cullen et al. 1999). The interaction of Zn (and Cd and Co) with $CO_2$ is an important area of future research, particularly in coastal environments. With the continuing rise in atmospheric and surface ocean $pCO_2$ levels, broader changes in the biogeochemical cycling of Zn and other bioavailable trace metals will likely occur within the oceans, influencing NPP and thus total ocean carbon storage capacity. These low $pCO_2$ conditions environments that routinely occur in numerous coastal environments globally should be further examined for Zn effects in addition to carbon uptake dynamics in different temperature environments (Tortell et al. 2008; Dai et al. 2022). While there are elaborate biochemical capabilities available to many marine algae for dealing with Zn scarcity (Kellogg et al. 2022a), our results suggest that the geographic extent of possible Zn/C co-limiting environments may further decrease in the coming decades with rising anthropogenic $CO_2$ emissions. Despite this, the biochemical demand for Zn in marine organisms remains substantial, with cellular demand rivaling that of Fe. The multitude of metabolic functions requiring Zn, including but not limited to carbonic anhydrase activity, implies the need for further exploration of Zn influences on primary productivity in a changing ocean environment.

## 5 Materials and Methods

### 5.1 Study area and sample collection

Sample collection occurred during the CICLOPS (Cobalamin and Iron Co-limitation of Phytoplankton Species) expedition (NBP18-01) aboard the RVIB *Nathaniel B. Palmer*, December 11, 2017 – March 3, 2018 in the Amundsen Sea and Ross Sea of the Southern Ocean (**Fig. 1a**). Station metadata is provided in **Supplementary Table 2.** All stations were assumed to be representative of TNB during this temporal study (as evident in the total dissolved metal, macronutrient, and chlorophyll *a* datasets). Water samples for dissolved trace metal analyses were collected using trace metal sampling protocols described previously (Cutter and Bruland 2012). A trace metal clean rosette suspended on a Kevlar line and equipped with twelve 8L X-Niskin bottles (Ocean Test Equipment) was used to collect seawater at depths ranging from 10 – 600 m. Niskin bottles were transported to a positive-pressure trace metal clean shipboard van for filtration upon surfacing. Total fluorescence on the vertical profiles was measured using an ECO chlorophyll fluorometer (Wet Labs) equipped to the rosette. The rosette also included instrumentation for measuring conductivity and temperature (Sea-Bird Electronics).

**5.2 Preparation of plasticware**

Polyethylene and polycarbonate sampling and incubation bottles were rigorously cleaned to remove trace metal contaminants before use. Bottles were rinsed with 18.2 Ω Milli-Q water (Millipore), soaked for 72h in <1% Citranox detergent, rotated, soaked for an additional 72h, and then rinsed five times with Milli-Q water. Bottles were then filled with 10% HCl (Baker instar-analyzed) by volume and soaked for a minimum of one week, rotated, and soaked for another week. Bottles were then rinsed five times with dilute acid (HCl, pH 2) and stored double-bagged in plastic zip bags. All cleaning work was conducted in a Class 100 clean room.

### 5.3 Underway seawater $pCO_2$ partial pressure

Surface water $pCO_2$ measurements were conducted aboard the RVIB *Nathaniel B. Palmer* using an underway method consisting of an air-water equilibrator and IR $CO_2$ analyzer developed and operated by the Lamont-Doherty Earth Observatory (LDEO) group (Takahashi et al. 2020). A complete data report and sensor list are available: https://service.rvdata.us/data/cruise/NBP1801/doc/NBP1801DATA.pdf (last access: 14 December 2024) (https://www.rvdata.us/, last access: 14 December 2024).

### 5.4 TDIC and POC measurements

Total alkalinity (TA) and dissolved inorganic carbon (DIC) were measured on CTD and incubations samples in near real-time aboard the NBP. Dissolved inorganic carbon (DIC) and total alkalinity (TA) samples were collected following the protocols of Dickson et. al 2007(Dickson et al. 2007). DIC analyses were conducted within ~4 h of collection. We acidified 1.25 mL of sample using an automated custom-built injection and bubble stripping system coupled to an infrared gas analyzer (LICOR LI7000) and integrated the infrared absorption signal versus time for each stripped gas sample to yield a total mass of $CO_2$. Each sample was analyzed in triplicate or greater. Since microbubbles regularly formed as samples warmed between sample acquisition and DIC analysis, every integration curve was visually inspected and those curves that exhibited evidence for bubbles were rejected. Certified reference materials (Dickson CRM batch 169) were analyzed between every 3 to 4 unknowns. The estimated precision based upon unknowns (>860 samples run in triplicate) and CRM replicates ($n = 738$) was $\pm$ 2.0 $\mu mol\ kg^{-1}$ ($\pm$1 SD). As described by DeJong et al. 2015(DeJong et al. 2015), analyses for TA on filtered samples were completed within ~12 h of collection by using a potentiometric

titrator (Metrohm 855 Robotic Titrosampler). The estimated precision based on replicate analyses of CRMs (n = 195) was ± 2.6 μmol $kg^{-1}$ (±1 SD).

### 5.5 Analysis of historical atmospheric and surface ocean $pCO_2$ trends

Decadal surface ocean $pCO_2$ reconstructions from Jiang et al. 2023 (Jiang et al. 2023) were downloaded, binned by decade, and plotted using the 'violinplot' in MATLAB. Atmospheric $pCO_2$ data was assembled from the running Mauna Loa record (Keeling et al. 1976), and from measurements made on Antarctic firn ice (Etheridge et al. 1996).

### 5.6 Calculation of Zn-and $pCO_2$ co-limitation of phytoplankton thresholds

There are few experimental measurements of Zn- and $pCO_2$-co-limitation, either in the lab or *in situ*. This study documented Zn of a natural phytoplankton assemblage in the field at a $pCO_2$ of ~220 ppm. In the literature, several models exist to interpret co-limitation (Buitenhuis et al. 2003; Saito et al. 2008). For this study we chose to use the biochemically dependent co-limitation model for growth rate (μ):

$$\mu = V_{max} \frac{[CO_{2(aq)}]}{\varphi K_s + [CO_{2(aq)}]}, \quad (1)$$

where $V_{max}$ is the maximum growth rate, $[CO_{2(aq)}]$ is the aqueous $CO_2$ concentration of the growth medium in micromoles per kilogram of seawater, $K_s$ is the half-saturation constant in micromoles per kilogram of seawater, and φ is a Zn-dependent growth term:

$$\varphi = \frac{[dZn] + K_{s,Zn}}{[dZn]} \quad (2)$$

Here, the dissolved Zn concentration in the growth medium [dZn] is modified by a Zn-dependent saturation constant ($K_{s,Zn}$). Few studies have enough experimental data to robustly establish a kinetic relationship between [dZn] and [$CO_{2(aq)}$], so we compiled several estimates for these terms from the literature. Diatom growth rates under $pCO_2$ limitation were taken from Riebesell et al. (1993) (Riebesell et al. 1993). Reported pH and temperature measurements for each treatment, a total alkalinity of 2300 μmol $kg^{-1}$, and a salinity of 35 were used to calculate aqueous $CO_2$ concentrations using CO2SYSv3.2.1.(Sharp et al. 2023). Reported $V_{max}$ and $K_s$ for *D. brightwellii, T. punctigera,* and *R. alata* were 1.46, 1.30, and 0.93 $d^{-1}$, and 1.4, 1.2, and 2.1 μmol $kg^{-1}$, respectively. Values for coccolithophore growth ($K_s$ = 0.97 μmol $kg^{-1}$, $V_{max}$ = 4.7 $d^{-1}$) were taken from Krumhardt et al. (2017) (Krumhardt et al. 2017). A value for $K_{s,Zn}$ of 300 pmol $L^{-1}$ was taken from Buitenhuis et al. (2003). This value is for the coccolithophore *E. huxleyii* generated under varying $CO_2$ and Zn conditions, and Zn response growth curves under single $CO_2$ conditions (ambient) are similar to other diatoms like *T. pseudonana*(Sunda and Huntsman 1995). The value of 300 pmol $L^{-1}$ appears high, but is tied to the functional form of the biochemically co-limitation equation(Buitenhuis et al. 2003; Saito et al. 2008). Based on the same dataset and different models for co-limitation, Buitenhuis et al. (2003) arrived at $K_{s,Zn}$ values of ranging from 38 pmol $L^{-1}$ to 300 pmol $L^{-1}$. They calculated Zn-limitation alone, at $CO_2$-replete conditions, of 19 pmol $L^{-1}$. Thus, the chosen value of $K_{s,Zn}$ is not a reflection of high Zn demand but determined by the functionality of biochemical co-limitation by Zn and C.

To calculate φ, a surface ocean Zn concentration of 50 pmol $L^{-1}$ was assumed (Bruland 1980; Wyatt et al. 2014). While these concentrations reflect total dissolved Zn, the relationship between bioavailable free Zn and dZn, especially in the field, remains unclear. Eq. 1 was then used to calculate effective $CO_2$ concentrations (and thus $pCO_2$ values) at which growth is halved,

or in other words, $\mu = 0.5V_{max}$. We note that this calculation is distinct from the $CO_2$ half-saturation constant because of the co-limitation by Zn. The median $pCO_2$ threshold for 50% growth from the three diatom species was 278 ppm. Including coccolithophores decreases the median to 259 ppm. These values are slightly higher than the *in situ* evidence for Zn limitation at 220 ppm presented in the present study. Our results cannot be considered as an upper bound for Zn-$CO_2$ limitation, but serve as evidence for growth limitation under those specific environmental conditions.

**5.7 Analyses of total dissolved metals using isotope dilution**

The analysis of total dissolved metals for this expedition has been described previously (Kell et al. 2024). Briefly, seawater collected shipboard by pressure-filtering X-Niskin bottles through an acid-washed 142 mm, 0.2 µM polyethersulfone Supor membrane filter (Pall) within 3 hours of rosette recovery using high purity (99.999%) $N_2$ gas and stored at 4ºC. All sample collection occurred shipboard within an on-deck trace metal clean van. Samples were acidified to pH 1.7 with high purity HCl (Optima) within 7 months of collection and were stored acidified at room temperature for over 1 year prior to analysis.

Quantification of total dissolved Fe, Mn, Ni, Cu, Zn, and Cd was performed using isotope dilution. Acidified seawater samples were spiked with a stable isotope spike solution artificially enriched in $^{57}Fe$, $^{61}Ni$, $^{65}Cu$, $^{67}Zn$, and $^{110}Cd$ (Oak Ridge National Laboratory). Concentrations and spike ratios were verified by ICP-MS using a multi-element standard curve (SPEX CertiPrep). Preconcentration of spiked seawater samples for total dissolved metal analysis was performed using the automated solid phase extraction system seaFAST-pico (Elemental Scientific) in offline concentration mode with an initial volume of 15mL and elution volume of

500µL (Rapp et al. 2017; Wuttig et al. 2019). Following preconcentration, multielemental quantitative analysis was performed using an iCAP-Q inductively coupled plasma-mass spectrometer (ICP-MS) (Thermo Scientific). Concentrations of Mn, Fe, Ni, Cu, Zn and Cd were determined using a six-point external standard curve of a multi-element standard (SPEX CertiPrep), diluted to range from 1-10 ppb in 5% nitric acid. An indium standard (SPEX CertiPrep) was similarly added to these standard stocks, diluted to range 1-10 ppb. Instrument injection blanks consisted of 5% nitric acid in Milli-Q. Standard curve $R^2$ values were ≥0.98 for all metals monitored. Method accuracy and precision were assessed using the 2009 GEOTRACES coastal surface seawater (GSC) standard (n = 8; **Supplementary Table 6**), which produced values consistent with consensus results (Kell et al. 2024).

**5.8 Macronutrient, pigment, and Fv/Fm analyses**

Seawater for macronutrient (silicate, phosphate, nitrate, and nitrite) analyses were filtered through 0.2 µm pore-size Supor membrane filters and frozen at sea in acid-washed 60-mL high-density polyethylene bottles until analysis. Macronutrient analyses were conducted by nutrient autoanalyzer (Technicon Autoanalyzer II) by Joe Jennings at Oregon State University. The chemotaxonomic distribution of phytoplankton pigments was determined using HPLC as described previously (DiTullio et al. 2003). Photosynthetic efficiency of photosystem II (Fv/Fm) was measured using a Phyto PAM phytoplankton analyzer (Walz, Effeltrich, Germany) as described previously (Schanke et al. 2021).

**5.9 Bacterial abundance**

One ml samples for heterotrophic prokaryotes abundance (HPA) analysis were fixed for 10 min with a mix of paraformaldehyde and glutaraldehyde (1% and 0.05% final concentration, respectively), frozen in liquid nitrogen and stored at −80°C until analysis. After thawing, samples were stained with SYBR Green (Invitrogen Milan, Italy) using $10^{-3}$ dilution of stock solution for 15 min at room temperature. Cell concentrations were assessed using a FACSVerse flow cytometer (BD BioSciences Inc., Franklin Lakes, USA) equipped with a 488 nm Ar laser and standard set of optical filters. FCS Express software was used for analyzing the data and HP were discriminated from other particles on the basis of scatter and green fluorescence from SYBR Green (Balestra et al. 2011).

**5.10 ICP-MS analysis and Zn uptake rates using $^{67}$Zn**

$^{67}$Zn stable isotope uptake experiments were performed to quantify the movement of dissolved Zn to the particulate phase (in units of pmol $L^{-1}$ $d^{-1}$), see (Kell et al. 2024). Briefly, unfiltered seawater was collected using the trace metal rosette over a depth range of 10 – 600 m into 250mL trace metal clean polycarbonate bottles. Bottles were spiked with $^{67}$Zn such that the total added (spiked) concentration of Zn was 2 nM. Immediately after spiking, incubation bottles were sealed, inverted to mix, and transferred to flow-through on-deck incubators for 24hr. Biomass was collected after 24hr by vacuum filtering each incubation sample at 34.5 kPa (5 psi) onto an acid-cleaned 3μm pore-size acrylic copolymer Versapore filter (Pall) mounted on an acid-cleaned plastic filtration rig. Sample filters were retrieved from storage at -80°C, removed from cryovials using plastic acid-washed forceps, and transferred into trace metal clean 15 mL PFA vials with 4 mL of 5% $HNO_3$ (Optima) containing a 1 ppb Indium (In) internal standard. Filters were digested for ~3.5h at 140°C using a HotBlock® heating block (Environmental

Express, USA) before they were removed and discarded. After evaporating the remaining solution to just dryness, the residue was resuspended in 2 mL of 5% $HNO_3$ (Optima) by light vortexing. Process blank filters were digested and processed as sample filters were. This experiment was also carried out using $^{110}Cd$ as a tracer of Cd uptake in separate incubation bottles (data not shown here). Digests were analyzed in duplicate by ICP-MS using a Thermo ICAP-Q plasma mass spectrometer calibrated to a multi-element standard curve (Spex Certiprep) over a range of 1 – 20 ppb. Natural Cd and Zn isotope abundances of the standards were assumed to calculate concentrations of $^{110}Cd$, $^{111}Cd$, $^{114}Cd$, $^{67}Zn$, $^{66}Zn$, and $^{68}Zn$. Total Zn uptake (pmol $L^{-1}$ $d^{-1}$) was calculated using particulate $^{67}Zn$ and total water column dZn measurements as described previously(Cox et al. 2014). The particulate metal measurements captured contributions from the active transport of metal into cells, nonspecific metal adsorption to cell surfaces, metal adsorption to non-living particulate organic matter, and metal adsorption to particulate inorganic matter, though we expect active transport into cells to dominate the measured particulate isotopic signal due to the high abundance of actively growing autotrophic cells in the photic zone observed in Southern Ocean during austral summer. Particulate Zn:P measurements were calculated using particulate Zn measured on Cd-spiked filters and thus do not include any pZn contribution from Zn tracer addition. Particulate phosphorus concentrations were measured by ICP-MS simultaneously and were calibrated to a standard curve ranging from 100 to 3200 ppb using a 1 ppm certified P stock (Alfa Aesar Specpure). All SPEX and P standard curves had $R^2$ values > 0.99. The Zn stock solution used in the incubation experiments was similarly analyzed by ICP-MS to confirm that the stock was not Fe contaminated— this analysis showed that less than 2.3 pM (which was near the instrument blank level for this

analysis) of iron was added for every 2 nM of zinc, far less than needed to stimulate phytoplankton to the extent observed in our experiments.

**5.11 Shipboard incubation experiments**

Incubation experiments were conducted at station 27 (-74.9870°N, 165.8898°E). Raw surface seawater was pumped directly into a cleanroom container van, collected into acid-cleaned 50L carboys, and dispensed into acid-washed 1L polycarbonate bottles using a trace metal sampling system with acid-washed polypropylene tubing and a teflon diaphragm pump. Incubation bottles were first rinsed with seawater then filled. Seawater was collected at 16:05 UTC. Triplicate incubation bottles were amended with +Fe (1 nM), +Zn (2 nM) and +Fe+Zn, sealed, and placed into a flow-through on-deck incubator with light screens that shaded the incubator to 20% percent ambient surface irradiance. Incubations were sampled at 0, 48, 96, and 144 hours (corresponding to T0, T2, T4, and T6 timepoints) for analysis by filtering onto GFF filters for chlorophyll (all time points, biological triplicates), pigment analyses (T6, biological triplicates), and proteomic analyses (T6, pooled biological triplicates). Chlorophyll was extracted immediately, otherwise samples were frozen at -80°C until further analyses, with pigment and protein samples kept in -80°C freezers, liquid nitrogen dewars, or dry ice coolers at all times during transport back to the laboratories. All amendments and sampling were conducted in a positive-pressure, clean room van with laminar flow hoods and plastic sheeting to minimize trace-metal contamination.

**5.12 Metaproteomic analysis**

Water column metaproteomic biomass was collected onto 0.2, 3, and 51 µm pore-size filters using in-situ battery operated McLane pumps. Incubation metaproteomic samples were collected onto GFF filters. Filters were frozen at -80°C and stored until laboratory extraction. Frozen filters were thawed and extracted as described previously (Hughes et al. 2014). Briefly, filters were extracted using SDS detergent to solubilize both membrane and soluble proteins and subjected to a 10-min heating incubation at 95 °C. Protein material was subsequently purified, alkylated, reduced and digested with trypsin (mass spectrometry grade; Promega Corporation) at a trypsin:protein ratio of 1:20 and peptides were purified using C18 tips (Pierce C18 Tips, 100-µl bed; Thermo Fisher Scientific). Purified peptides were diluted to 0.1 µg $\mu l^{-1}$ and 20 µl (2 µg) was injected onto a Dionex UltiMate 3000 RSLCnano LC system (Thermo Fisher Scientific) with an additional RSLCnano pump run in online two-dimensional active modulation mode coupled to a Thermo Fusion Orbitrap mass spectrometer.

A translated metatranscriptome (see below) was used as a reference protein database and peptide spectra matches were performed using the SEQUEST algorithm within Proteome Discoverer v.2.1 (Thermo Fisher Scientific) with a fragment tolerance of 0.6 Da and parent tolerance of 10 ppm. Identification criteria consisted of a peptide threshold of 95% (false discovery rate (FDR) = 0.1%) and protein threshold of 99% (1 peptide minimum, FDR = 0.8%) in Scaffold v.5 (Proteome Software) resulting in 5,387 proteins identified in the incubation experiment and 27,924 proteins identified in the water column. To avoid double-counting mass spectra, exclusive spectral counts were used for the downstream proteomic analysis. Exclusive spectral counts were normalized using the normalized spectral abundance factor (NSAF) calculation (Zhang et al. 2010) to allow for a comparison of protein abundance across samples while remaining consistent with the metatranscriptomic procedure, see Cohen et al. 2021 for

details. Counts associated with redundant ORFs (sharing identical taxonomic and functional assignments) were summed together. The stand-alone command line application BLAST+ from the National Center for Biotechnology Information (NCBI) was used to identify proteins of interest in the metaproteomic data. Metaproteomes were BLAST searched (E = 5e-5) against the known sequences of proteins of interest acquired from annotated proteomic databases **(Supplementary Table 4)** and combined with further annotation data based on contig ID (see below).

**5.13 Metatranscriptomic analysis**

RNA sequencing was performed using the Illumina HiSeq platform. Transcriptomic assemblies were generated for biomass collected using McLane pumps filtered through 0.2, 3, and 51 μm pore-size filters. In order to enrich metatranscriptomic libraries derived from 0.2 μm filters in prokaryotic transcripts and libraries derived from 3 μm and 51 μm filters in eukaryotic transcripts, 0.2 μm libraries were generated from total rRNA-depleted mRNA and 3 μm and 51 μm libraries were generated from polyA mRNA. Total RNA was extracted from 0.2 μm, 3 μm, and 51μm filters using Macherey-Nagel a NucleoMag RNA kit (Macherey-Nagel GmbH & Co.KG). Cleared lysate was loaded into a 96 deep-well plate and put on an epMotion 5075 TMX liquid handler to complete the RNA extraction following the Machery-Nagel standard protocol. For 3 μm and 51 μm samples with total RNA greater than 1 μg, 800 ng of total RNA was used for preparing poly A libraries with an Illumina Stranded mRNA Prep Ligation kit (Illumina), following the manufacturer's protocol. For the 3 μm and 51 μm samples with total RNA less than 1 μg, 20 ng of total RNA was used as input for the SMART-Seq v4 Ultra Low Input RNA kit (Takara Bio USA. Inc), which converts poly(A) RNA to full-length cDNA using a modified

oligo (dT) primer with simultaneous cDNA amplification. The resulting double-stranded cDNA was then fragmented using a Covaris E210 system with the target size of 300bp. Libraries were prepared from fragmented double-stranded cDNA using an Illumina Stranded mRNA Prep Ligation kit (Illumina). For RNA obtained from 0.2 μm filters, ribosomal RNA was removed using a riboPOOL Seawater Kit (Galen Laboratory Supplies, North Haven, Connecticut, USA). The riboPOOL Seawater Kit is a customized mixture of Removal Solutions: Pan-Prokaryote riboPOOL, Pan-Plant riboPOOL and Pan-Mammal in a ratio of 6:1:1. The rRNA-depleted total RNA was used for cDNA synthesis by Ovation RNA-Seq System V2 (TECAN, Redwood City, USA). Double stranded cDNA was then prepared for the libraries using an Illumina Stranded mRNA Prep Ligation kit (Illumina). Ampure XP beads (Beckman Coulter) were used for final library purification. Library quality was analyzed on a 2200 TapeStation System with an Agilent High Sensitivity DNA 1000 ScreenTape System (Agilent Technologies, Santa Clara, CA, USA). Resulting libraries were subjected to paired-end Illumina sequencing via NovaSeq S4.

The input paired-end fastq sequences are trimmed of sequencing adapters, primers and low quality bases by using either BLASTN (NCBI, v2.2.25) (Altschul et al. 1990) or trimmomatic, v0.36 (Bolger et al. 2014). The trimmed paired and unpaired sequences were then depleted of rRNA sequences with riboPicker v0.4.3 (Schmieder et al. 2012). The command-line program clc_assembler, v5.2.1 (Qiagen) was used to assemble processed sequences into contigs and ORFs were identified by FragGeneScan, v1.31 (Rho et al. 2010). The trimmed sequences were mapped to the predicted ORFs using the command-line program clc_mapper, v5.2.1 (Qiagen) to generate mapped raw read counts for each ORF. The raw counts were normalized initially to RPKM values, to account for variations in inter-sample sequencing depth and the ORF sequence length (Mortazavi et al. 2008). The RPKM values were subsequently converted to

TPM (transcripts per million) units for estimation of the relative RNA abundance among samples (Li and Dewey 2011). The ORFs were annotated for putative function by several programs in parallel using BLASTP against PhyloDB, hidden Markov models PFAM and TIGRFAM by HMMER, v3.3.2 (Eddy 2011), KEGG Ortholog HMM by kofamscan, v1.3.0 (Aramaki et al. 2020), and transmembrane HMM by TMHMM (Krogh et al. 2001). Additional annotations were generated by similarity searches using BLASTP to transporter (PhyloDB), organelle (PhyloDB) and KOG (Tatusov et al. 2003) databases. The ORFs are assigned to the best taxonomic species/group as determined by LPI (Lineage Probability Index) analysis (Podell and Gaasterland 2007). The final list of curated ORFs was generated by removing ORFs with low mapping coverage (< 50 reads total over all samples) and with no BLAST hits and no known domains.

**5.14 Statistical analysis and data visualization**

ANOVA and Dunnett tests were performed using MATLAB 2019a. Statistics are summarized in **Supplementary Table 3**. Figures were made using matplotlib (version 3.5.0), Ocean Data View (version 5.5.2), Excel (2019), and RStudio (version 1.3.1093). Color palettes used in Ocean Data View section plots (https://doi.org/10.5281/zenodo.1243862) are inverse "roma" for trace metal concentrations, "thermal" for Zn and Cd uptake rates, and "algae" for chlorophyll fluorescence (Crameri 2023).

**Data Availability**

CICLOPS (NBP18-01) conductivity–temperature–depth (CTD) hydrography data including pressure, temperature, total dissolved oxygen, conductivity, fluorescence, and beam

transmission (https://doi.org/10.1575/1912/bco-dmo.783911.1) and total dissolved metal, Zn and Cd uptake rate, macronutrient, and pigment datasets are available through the NSF Biological and Chemical Oceanography Data Management Office (BCO-DMO) repository (https://doi.org/10.7284/907753). Underway $pCO_2$ data collected during cruise NBP1801 are available through R2R at https://doi.org/10.7284/139318. The mass spectrometry global proteomics data for CICLOPS bottle incubations and water column analyses have been deposited with the ProteomeXchange Consortium through the PRIDE repository under the project name "Zinc-iron co-limitation of natural marine phytoplankton assemblages in coastal Antarctica" with project accession number PXD037056 (https://www.ebi.ac.uk/pride/archive/projects/PXD037056). This data is accessible for review by using the following login information: username reviewer_pxd037056@ebi.ac.uk, password: lFdOUoEb. The translated transcriptome used for spectrum to peptide matching has been deposited in the National Center for Biotechnology Information sequence read archive under BioProject accession no. PRJNA890306 (https://www.ncbi.nlm.nih.gov/bioproject/?term=PRJNA890306) and RNA-Seq BioSample accession nos. SAMN31286421-SAMN31286522 (https://www.ncbi.nlm.nih.gov/biosample/?term=SAMN31286421).

**Acknowledgements**

We thank the captain, crew, marine technicians and science party of RVIB Nathaniel B. Palmer for their support and contributions to the success of the NBP18-01 cruise. We thank Natalie Cohen for assistance and training with the SeaFAST. We thank Veronique Oldham for assistance with trace metal sampling. This work was funded by the National Science Foundation

(2125063, 1643684, 1924554) and the Simons Foundation to M.A.S.; NSF-PLR 1643845 to R.B.D, NSF-CO (2123055) to M.A.S. and A.V.S., and the National Institutes of Health (GM135709-01A1 to M.A.S).

**Author contributions statement**

All authors contributed to data acquisition and analysis. RMK, NLS, LEL, RJC, DR, DMM, MRM, FB, RBD, GRD and MAS implemented the shipboard incubation study. RMK, MMB, RJC, DR, TJH, and AVS contributed to the formal analysis. NLS, LEL, FB, OM, RF, and GRD contributed to pigment datasets and interpretations. CB provided bacterial abundance data. RBD contributed DIC and *in situ* $pCO_2$ data. AVS contributed analyses and discussion regarding historical $pCO_2$ data and Zn-C growth limitation estimates. AEA contributed the metatranscriptome reference database used for proteomic analyses. RMK and MAS wrote the original draft. RMK, MAS, GRD, AVS, TJH, and RBD contributed to review and editing. All authors approved the final submitted manuscript.

**Competing interests statement**

The authors declare no competing interests.

## Figures

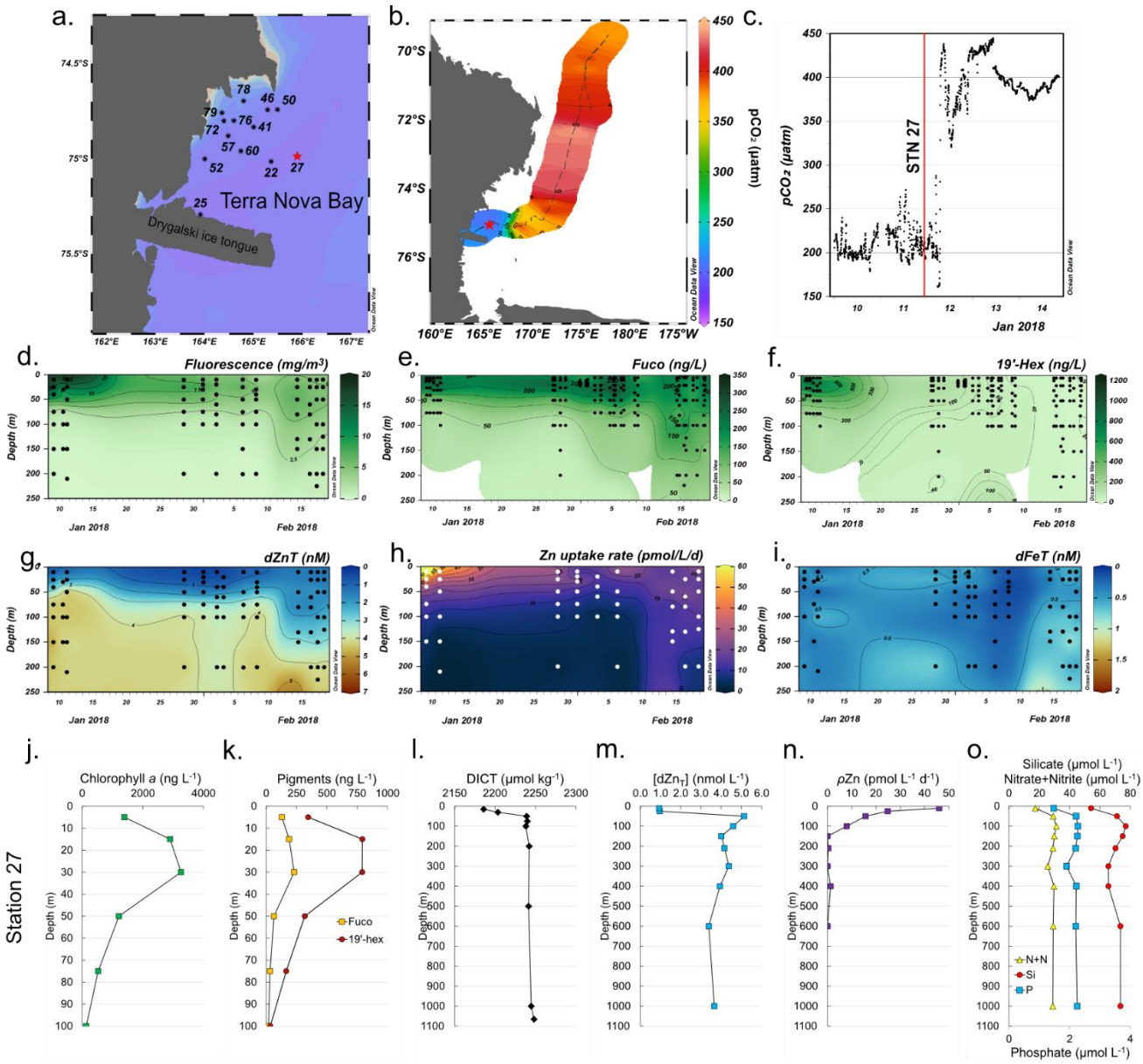


**Figure 1**. **Temporal biogeochemistry of Terra Nova Bay and characterization of the experimental site at Station 27.** (**a**) Sampling locations over the Ross Sea shelf in Terra Nova Bay, Antarctica. (**b**) Location of station 27 (red star) and surrounding seawater $pCO_2$ measured over a three-day transit northwards represented in color scale. (**c**) $pCO_2$ measured over time within TNB during the three-day transit shown in (b). The vertical red line denotes the $pCO_2$ level at the time of initial seawater collection at station 27. (**d**) Total chlorophyll fluorescence, (**e**) fucoxanthin (fuco), (**f**) 19' hexanoyloxyfucoxanthin (19'-hex), (**g**) total dissolved Zn, (**h**) total Zn uptake rates, and (**i**) total dissolved Fe measured in the upper 250 m represented on a color scale. Station data is presented in order of sampling date, from the earliest (Stn 22, early January) to the latest (Stn 79, late February). The data gap between January 13-23 occurred when the ship was unable to sample due to icebreaking duties for the McMurdo Station resupply ship. Stations

indicated in (a) are those where the trace metal rosette (TMR) was deployed; pigment data was supplemented with additional TNB stations using a CTD (Table S2). Depth profiles of (**j**) chlorophyll a, (**k**) the pigments fuco and 19'hex, (**l**) total dissolved inorganic carbon (DICT), (**m**) total dissolved Zn, (**n**) total Zn uptake rates, and (**o**) the macronutrients nitrate+nitrite (N+N), phosphate (P), and silicate (Si) at the study site. Panels (**d**),(**g**),(**h**) and (**i**) were originally presented in Kell et al. (2024) and are reprised here to introduce the environmental context of the study site.

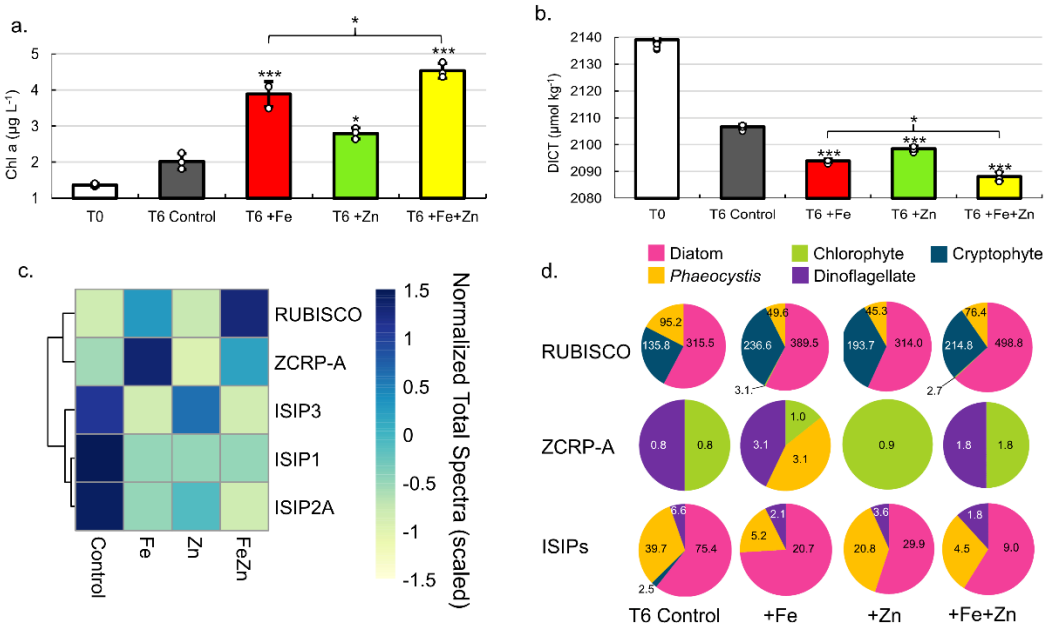


**Figure 2. Evidence for Zn co-limitation with Fe in bottle incubations.** (**a**) Chlorophyll *a* and (**b**) total DIC (DICT) at T0 (day 0) and in each treatment at T6 (day 6). Significant differences among groups were found using one-way ANOVA and post-hoc Dunnett test (*** $p < 0.001$, ** $p < 0.01$, * $p < 0.05$). Error bars are the standard deviation of biological triplicates (n=3). Individual data points are overlaid (white circles). (**c**) Heatmap of row-scaled exclusive protein spectral counts (normalized total spectra) showing relative protein abundance in each treatment. The dendrogram shows similarity in spectral abundance among samples based on Euclidean distance and hierarchical clustering. Color gradients represent low (yellow) to high (blue) protein expression. Ribulose-1,5-biphosphate carboxylase/oxygenase (RUBISCO), zinc/cobalt responsive protein A (ZCRP-A), and iron starvation induced proteins (ISIP1, ISIP2A, ISIP3) are shown. (**d**) Taxonomies assigned to RUBISCO, ZCRP-A, and ISIP proteins in each treatment at T6. Counts (normalized total spectra) assigned to each taxa are shown. ISIPs are the combined spectral counts of ISIP1A, ISIP2A and ISIP3.

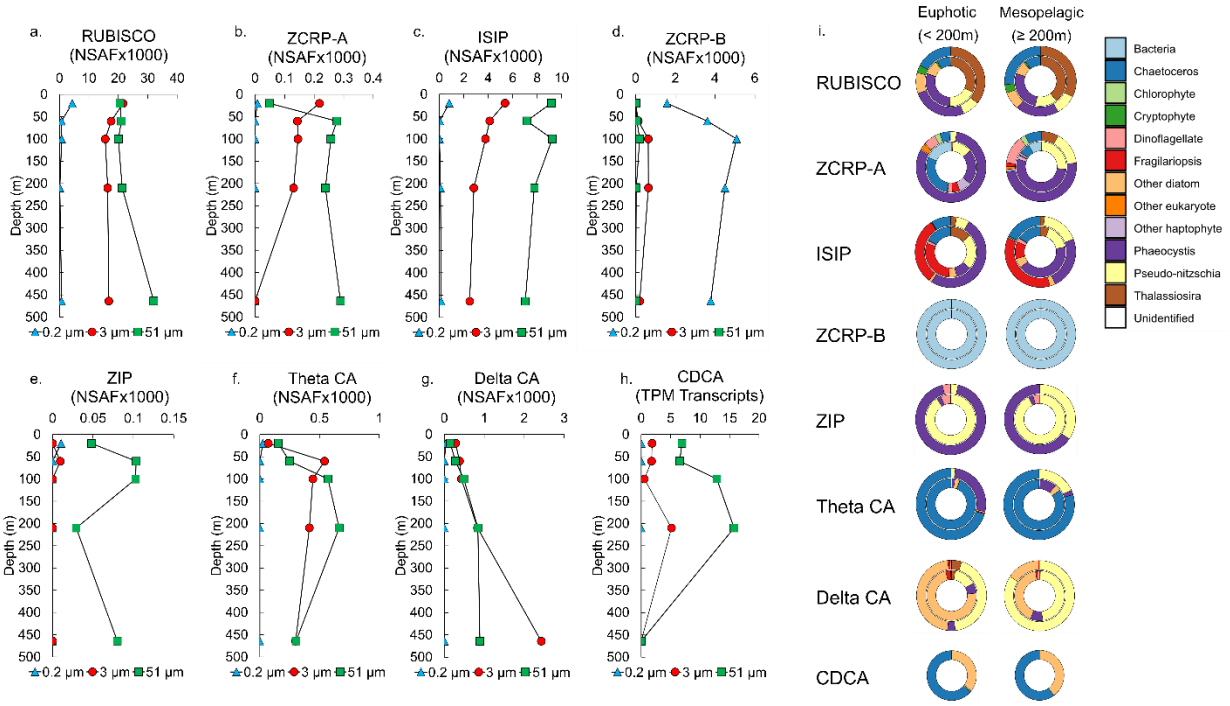


**Figure 3. Metatranscriptomic and metaproteomic detection of Zn- and Fe-related proteins of interest at the experimental site**. Depth profiles of summed NSAF-normalized protein spectral counts of (**a**) RUBISCO, (**b**) ZCRP-A, (**c**) iron starvation induced proteins (ISIPs), (**d**) ZCRP-B, (**e**) ZIP, (**f**) Theta CA, and (**g**) Delta CA detected from proteomic analysis of each filter size fraction (0.2, 3 and 51µm). (**h**) TPM-normalized transcript read counts of CDCA. (**i**) Stacked pie charts depicting relative community composition for proteins of interest for euphotic (< 200 m) and mesopelagic (≥ 200 m) depths. The outer rings show community composition based on NSAF-normalized protein spectral counts while the inner rings are TPM-normalized transcript read counts. Protein and transcript counts plotted in (**i**) were summed across all size fractions. ISIPs are the combined spectral counts of ISIP1A, ISIP2A and ISIP3.

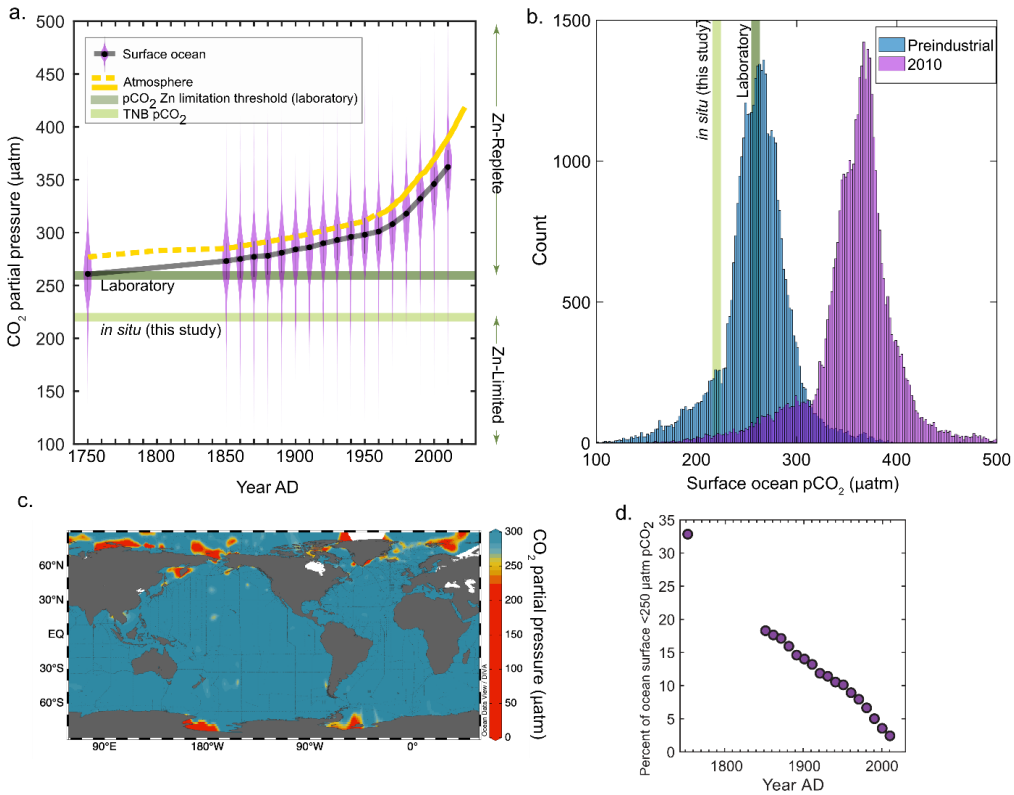


**Figure 4**. **The partial pressure of $CO_2$ ($pCO_2$) and associated phytoplankton responses from this study and the literature**. **(a)** Pre-industrial and decadal surface ocean $pCO_2$ reconstructions plotted as violin plots, with a running black line through the median values. The atmospheric curve is a composite of ice core data (dashed yellow line (Etheridge et al. 1996)) and the Mauna Loa record (solid yellow line (Keeling et al. 1976)). An estimated thresholds for zinc-limited growth is plotted as the median of previous laboratory results (259 µatm, dark green line; see Methods), and is compared to the *in situ* results of this study (220 µatm, light green line). **(b)** Data in (a) plotted as a histogram comparing preindustrial and modern (2010) $pCO_2$ values, with the same pCO2 levels indicated. (**c**) Global map of surface ocean $pCO_2$ plotted using GLODAPv2.2022 data (Lauvset et al. 2022). **(b)** Percentage of the ocean surface less than 250 µatm $pCO_2$ as a function of time. Surface ocean $pCO_2$ reconstructions taken from Jiang et al. 2023.

## References


Allen, A. E. and others. 2008. Whole-cell response of the pennate diatom Phaeodactylum tricornutum to iron starvation. Proc. Natl. Acad. Sci. **105**: 10438–10443. doi:10.1073/pnas.0711370105

Altschul, S. F., W. Gish, W. Miller, E. W. Myers, and D. J. Lipman. 1990. Basic local alignment search tool. J. Mol. Biol. doi:10.1016/S0022-2836(05)80360-2

Aramaki, T., R. Blanc-Mathieu, H. Endo, K. Ohkubo, M. Kanehisa, S. Goto, and H. Ogata. 2020. KofamKOALA: KEGG Ortholog assignment based on profile HMM and adaptive score threshold A. Valencia [ed.]. Bioinformatics **36**: 2251–2252. doi:10.1093/bioinformatics/btz859

Arrigo, K. R., K. E. Lowry, and G. L. van Dijken. 2012. Annual changes in sea ice and phytoplankton in polynyas of the Amundsen Sea, Antarctica. Deep Sea Res. Part II Top. Stud. Oceanogr. **71–76**: 5–15. doi:10.1016/j.dsr2.2012.03.006

Baars, O., and P. L. Croot. 2011. The speciation of dissolved zinc in the Atlantic sector of the Southern Ocean. Deep Sea Res. Part II Top. Stud. Oceanogr. **58**: 2720–2732. doi:10.1016/j.dsr2.2011.02.003

Balestra, C., L. Alonso-Sáez, J. M. Gasol, and R. Casotti. 2011. Group-specific effects on coastal bacterioplankton of polyunsaturated aldehydes produced by diatoms. Aquat. Microb. Ecol. doi:10.3354/ame01486

Behnke, J., and J. LaRoche. 2020. Iron uptake proteins in algae and the role of Iron Starvation-Induced Proteins (ISIPs). Eur. J. Phycol. **55**: 339–360. doi:10.1080/09670262.2020.1744039

Bender, S. J. and others. 2018. Colony formation in Phaeocystis antarctica: connecting molecular mechanisms with iron biogeochemistry. Biogeosciences **15**: 4923–4942. doi:10.5194/bg-15-4923-2018

Bolger, A. M., M. Lohse, and B. Usadel. 2014. Trimmomatic: a flexible trimmer for Illumina sequence data. Bioinformatics **30**: 2114–2120. doi:10.1093/bioinformatics/btu170

Bruland, K. W. 1980. Oceanographic distributions of cadmium, zinc, nickel, and copper in the North Pacific. Earth Planet. Sci. Lett. **47**: 176–198. doi:10.1016/0012-821X(80)90035-7

Bruland, K. W. 1989. Complexation of zinc by natural organic ligands in the central North Pacific. Limnol. Oceanogr. **34**: 269–285. doi:10.4319/lo.1989.34.2.0269

Buitenhuis, E. T., K. R. Timmermans, and H. J. W. de Baar. 2003. Zinc-bicarbonate colimitation of Emiliania huxleyi. Limnol. Oceanogr. **48**: 1575–1582. doi:10.4319/lo.2003.48.4.1575

Chavez, F. P., J. Sevadjian, C. Wahl, J. Friederich, and G. E. Friederich. 2018. Measurements of pCO2 and pH from an autonomous surface vehicle in a coastal upwelling system. Deep Sea Res. Part II Top. Stud. Oceanogr. **151**: 137–146. doi:10.1016/j.dsr2.2017.01.001

Coale, K. H., X. Wang, S. J. Tanner, and K. S. Johnson. 2003. Phytoplankton growth and biological response to iron and zinc addition in the Ross Sea and Antarctic Circumpolar Current along 170°W. Deep Sea Res. Part II Top. Stud. Oceanogr. **50**: 635–653. doi:10.1016/S0967-0645(02)00588-X

Cox, A. D., A. E. Noble, and M. A. Saito. 2014. Cadmium enriched stable isotope uptake and addition experiments with natural phytoplankton assemblages in the Costa Rica Upwelling Dome. Mar. Chem. **166**: 70–81. doi:10.1016/j.marchem.2014.09.009

Crameri, F. 2023. Scientific colour maps.doi:10.5281/ZENODO.1243862

Crawford, D. W. and others. 2003. Influence of zinc and iron enrichments on phytoplankton growth in the northeastern subarctic Pacific. Limnol. Oceanogr. **48**: 1583–1600. doi:10.4319/lo.2003.48.4.1583

Cullen, J. T., T. W. Lane, F. M. M. Morel, and R. M. Sheerell. 1999. Modulation of cadmium uptake in phytoplankton by seawater CO2 concentration. Nature. doi:10.1038/46007

Cutter, G. A., and K. W. Bruland. 2012. Rapid and noncontaminating sampling system for trace elements in global ocean surveys. Limnol. Oceanogr. Methods. doi:10.4319/lom.2012.10.425

Dai, M. and others. 2022. Carbon Fluxes in the Coastal Ocean: Synthesis, Boundary Processes, and Future Trends. Annu. Rev. Earth Planet. Sci. **50**: 593–626. doi:10.1146/annurev-earth-032320-090746

DeJong, H. B., R. B. Dunbar, D. Mucciarone, and D. A. Koweek. 2015. Carbonate saturation state of surface waters in the Ross Sea and Southern Ocean: controls and implications for the onset of aragonite undersaturation. Biogeosciences **12**: 6881–6896. doi:10.5194/bg-12-6881-2015

Dickson, A. G., C. L. Sabine, and J. R. Christian,. 2007. Guide to best practices for ocean CO2 measurement. North Pacific Marine Science Organization.

DiTullio, G. R. and others. 2000. Rapid and early export of Phaeocystis antarctica blooms in the Ross Sea, Antarctica. Nature. doi:10.1038/35007061

DiTullio, G. R., N. Garcia, S. F. Riseman, and P. N. Sedwick. 2007. Effects of iron concentration on pigment composition in Phaeocystis antarctica grown at low irradiance. Biogeochemistry **83**: 71–81. doi:10.1007/s10533-007-9080-8

DiTullio, G. R., M. E. Geesey, A. Leventer, and M. P. Lizotte. 2003. Algal pigment ratios in the Ross Sea: Implications for Chemtax analysis of Southern Ocean data, p. 35–51. *In*.

DiTullio, G. R., and W. O. Smith. 1996. Spatial patterns in phytoplankton biomass and pigment distributions in the Ross Sea. J. Geophys. Res. Oceans **101**: 18467–18477. doi:10.1029/96JC00034

Dreux Chappell, P., J. Vedmati, K. E. Selph, H. A. Cyr, B. D. Jenkins, M. R. Landry, and J. W. Moffett. 2016. Preferential depletion of zinc within Costa Rica upwelling dome creates conditions for zinc co-limitation of primary production. J. Plankton Res. **38**: 244–255. doi:10.1093/plankt/fbw018

Eddy, S. R. 2011. Accelerated Profile HMM Searches W.R. Pearson [ed.]. PLoS Comput. Biol. **7**: e1002195. doi:10.1371/journal.pcbi.1002195

Ellwood, M. J. 2004. Zinc and cadmium speciation in subantarctic waters east of New Zealand. Mar. Chem. doi:10.1016/j.marchem.2004.01.005

Etheridge, D. M., L. P. Steele, R. L. Langenfelds, R. J. Francey, J.-M. Barnola, and V. I. Morgan. 1996. Natural and anthropogenic changes in atmospheric $CO_2$ over the last 1000 years from air in Antarctic ice and firn. J. Geophys. Res. Atmospheres **101**: 4115–4128. doi:10.1029/95JD03410

Fitzwater, S. E., K. S. Johnson, R. M. Gordon, K. H. Coale, and W. O. Smith. 2000. Trace metal concentrations in the Ross Sea and their relationship with nutrients and phytoplankton growth. Deep-Sea Res. Part II Top. Stud. Oceanogr. **47**: 3159–3179. doi:10.1016/S0967-0645(00)00063-1

Fourquez, M., M. Bressac, S. L. Deppeler, M. Ellwood, I. Obernosterer, T. W. Trull, and P. W. Boyd. 2020. Microbial Competition in the Subpolar Southern Ocean: An Fe–C Co-limitation Experiment. Front. Mar. Sci. **6**: 776. doi:10.3389/fmars.2019.00776

Franck, V., K. Bruland, D. Hutchins, and M. Brzezinski. 2003. Iron and zinc effects on silicic acid and nitrate uptake kinetics in three high-nutrient, low-chlorophyll (HNLC) regions. Mar. Ecol. Prog. Ser. **252**: 15–33. doi:10.3354/meps252015

Harrison, C. S., M. C. Long, N. S. Lovenduski, and J. K. Moore. 2018. Mesoscale Effects on Carbon Export: A Global Perspective. Glob. Biogeochem. Cycles **32**: 680–703. doi:10.1002/2017GB005751

Hughes, C. S., S. Foehr, D. A. Garfield, E. E. Furlong, L. M. Steinmetz, and J. Krijgsveld. 2014. Ultrasensitive proteome analysis using paramagnetic bead technology. Mol. Syst. Biol. **10**: 757. doi:10.15252/msb.20145625

Jakuba, R. W., M. A. Saito, J. W. Moffett, and Y. Xu. 2012. Dissolved zinc in the subarctic North Pacific and Bering Sea: Its distribution, speciation, and importance to primary producers. Glob. Biogeochem. Cycles. doi:10.1029/2010GB004004

Jensen, E. L., S. C. Maberly, and B. Gontero. 2020. Insights on the Functions and Ecophysiological Relevance of the Diverse Carbonic Anhydrases in Microalgae. Int. J. Mol. Sci. **21**: 2922. doi:10.3390/ijms21082922

Jiang, L. and others. 2023. Global Surface Ocean Acidification Indicators From 1750 to 2100. J. Adv. Model. Earth Syst. **15**: e2022MS003563. doi:10.1029/2022MS003563

Keeling, C. D., R. B. Bacastow, A. E. Bainbridge, C. A. Ekdahl, P. R. Guenther, L. S. Waterman, and J. F. S. Chin. 1976. Atmospheric carbon dioxide variations at Mauna Loa

Observatory, Hawaii. Tellus Dyn. Meteorol. Oceanogr. **28**: 538. doi:10.3402/tellusa.v28i6.11322

Kell, R. M. and others. 2024. High metabolic zinc demand within native Amundsen and Ross sea phytoplankton communities determined by stable isotope uptake rate measurements. Biogeosciences **21**: 5685–5706. doi:10.5194/bg-21-5685-2024

Kellogg, R. M. and others. 2022a. Adaptive responses of marine diatoms to zinc scarcity and ecological implications. Nat. Commun. 2022 131 **13**: 1–13. doi:10.1038/s41467-022-29603-y

Kellogg, R. M., M. R. McIlvin, J. Vedamati, B. S. Twining, J. W. Moffett, A. Marchetti, D. M. Moran, and M. A. Saito. 2020. Efficient zinc/cobalt inter-replacement in northeast Pacific diatoms and relationship to high surface dissolved Co : Zn ratios. Limnol. Oceanogr. **65**: 2557–2582. doi:10.1002/lno.11471

Kellogg, R. M., D. M. Moran, M. R. McIlvin, A. V. Subhas, A. E. Allen, and M. A. Saito. 2022b. Lack of a Zn/Co substitution ability in the polar diatom *Chaetoceros neogracile* RS19. Limnol. Oceanogr. **67**: 2265–2280. doi:10.1002/lno.12201

Krogh, A., B. Larsson, G. von Heijne, and E. L. L. Sonnhammer. 2001. Predicting transmembrane protein topology with a hidden markov model: application to complete genomes11Edited by F. Cohen. J. Mol. Biol. **305**: 567–580. doi:10.1006/jmbi.2000.4315

Krumhardt, K. M., N. S. Lovenduski, M. D. Iglesias-Rodriguez, and J. A. Kleypas. 2017. Coccolithophore growth and calcification in a changing ocean. Prog. Oceanogr. **159**: 276–295. doi:10.1016/j.pocean.2017.10.007

Lane, T. W., and F. M. Morel. 2000a. A biological function for cadmium in marine diatoms. Proc. Natl. Acad. Sci. U. S. A. **97**: 4627–31. doi:10.1073/pnas.090091397

Lane, T. W., and F. M. M. Morel. 2000b. Regulation of Carbonic Anhydrase Expression by Zinc, Cobalt, and Carbon Dioxide in the Marine Diatom Thalassiosira weissflogii. Plant Physiol. **123**: 345–352. doi:10.1104/pp.123.1.345

Lauvset, S. K. and others. 2022. GLODAPv2.2022: the latest version of the global interior ocean biogeochemical data product. Earth Syst. Sci. Data **14**: 5543–5572. doi:10.5194/essd-14-5543-2022

Lhospice, S. and others. 2017. Pseudomonas aeruginosa zinc uptake in chelating environment is primarily mediated by the metallophore pseudopaline. Sci. Rep. **7**: 17132. doi:10.1038/s41598-017-16765-9

Li, B., and C. N. Dewey. 2011. RSEM: accurate transcript quantification from RNA-Seq data with or without a reference genome. BMC Bioinformatics **12**: 323. doi:10.1186/1471-2105-12-323

Lohan, M. C., P. J. Statham, and D. W. Crawford. 2002. Total dissolved zinc in the upper water column of the subarctic North East Pacific. Deep Sea Res. Part II Top. Stud. Oceanogr. **49**: 5793–5808. doi:10.1016/S0967-0645(02)00215-1

Mangoni, O., M. Saggiomo, F. Bolinesi, M. Castellano, P. Povero, V. Saggiomo, and G. R. DiTullio. 2019. Phaeocystis antarctica unusual summer bloom in stratified antarctic coastal waters (Terra Nova Bay, Ross Sea). Mar. Environ. Res. doi:10.1016/j.marenvres.2019.05.012

Martin, J. H., S. E. Fitzwater, and R. M. Gordon. 1990. Iron deficiency limits phytoplankton growth in Antarctic waters. Glob. Biogeochem. Cycles **4**: 5–12. doi:10.1029/GB004i001p00005

Mazzotta, M. G., M. R. McIlvin, D. M. Moran, D. T. Wang, K. D. Bidle, C. H. Lamborg, and M. A. Saito. 2021. Characterization of the metalloproteome of Pseudoalteromonas (BB2-AT2): biogeochemical underpinnings for zinc, manganese, cobalt, and nickel cycling in a ubiquitous marine heterotroph. Metallomics **13**. doi:10.1093/mtomcs/mfab060

Middag, R., H. J. W. De Baar, and K. W. Bruland. 2019. The Relationships Between Dissolved Zinc and Major Nutrients Phosphate and Silicate Along the GEOTRACES GA02 Transect in the West Atlantic Ocean. Glob. Biogeochem. Cycles **33**: 63–84. doi:10.1029/2018GB006034

Milner, M. J., J. Seamon, E. Craft, and L. V. Kochian. 2013. Transport properties of members of the ZIP family in plants and their role in Zn and Mn homeostasis. J. Exp. Bot. **64**: 369–381. doi:10.1093/jxb/ers315

Moore, C. M. and others. 2013. Processes and patterns of oceanic nutrient limitation. Nat. Geosci. **6**: 701–710. doi:10.1038/ngeo1765

Morel, F. M. M., J. R. Reinfelder, S. B. Roberts, C. P. Chamberlain, J. G. Lee, and D. Yee. 1994. Zinc and carbon co-limitation of marine phytoplankton. Nature **369**: 740–742. doi:10.1038/369740A0

Mortazavi, A., B. A. Williams, K. McCue, L. Schaeffer, and B. Wold. 2008. Mapping and quantifying mammalian transcriptomes by RNA-Seq. Nat. Methods **5**: 621–628. doi:10.1038/nmeth.1226

Obernosterer, I., M. Fourquez, and S. Blain. 2015. Fe and C co-limitation of heterotrophic bacteria in the naturally fertilized region off the Kerguelen Islands. Biogeosciences **12**: 1983–1992. doi:10.5194/bg-12-1983-2015

Podell, S., and T. Gaasterland. 2007. DarkHorse: a method for genome-wide prediction of horizontal gene transfer. Genome Biol. **8**: R16. doi:10.1186/gb-2007-8-2-r16

Rapp, I., C. Schlosser, D. Rusiecka, M. Gledhill, and E. P. Achterberg. 2017. Automated preconcentration of Fe, Zn, Cu, Ni, Cd, Pb, Co, and Mn in seawater with analysis using high-resolution sector field inductively-coupled plasma mass spectrometry. Anal. Chim. Acta. doi:10.1016/j.aca.2017.05.008

Redfield, A. C. 1958. The Biological Control of Chemical Factors in the Environment. Am. Sci. doi:10.2307/27828530

Rho, M., H. Tang, and Y. Ye. 2010. FragGeneScan: predicting genes in short and error-prone reads. Nucleic Acids Res. **38**: e191–e191. doi:10.1093/nar/gkq747

Riebesell, U., D. A. Wolf-Gladrow, and V. Smetacek. 1993. Carbon dioxide limitation of marine phytoplankton growth rates. Nature **361**: 249–251. doi:10.1038/361249a0

Robbins, L. L. and others. 2018. Spatial and Temporal Variability of $pCO_2$ , Carbon Fluxes, and Saturation State on the West Florida Shelf. J. Geophys. Res. Oceans **123**: 6174–6188. doi:10.1029/2018JC014195

Saito, M. A., and T. J. Goepfert. 2008. Zinc-cobalt colimitation of *Phaeocystis antarctica*. Limnol. Oceanogr. **53**: 266–275. doi:10.4319/lo.2008.53.1.0266

Saito, M. A., T. J. Goepfert, and J. T. Ritt. 2008. Some thoughts on the concept of colimitation: Three definitions and the importance of bioavailability. Limnol. Oceanogr. **53**: 276–290. doi:10.4319/lo.2008.53.1.0276

Schanke, N. L., F. Bolinesi, O. Mangoni, C. Katlein, P. Anhaus, M. Hoppmann, P. A. Lee, and G. R. DiTullio. 2021. Biogeochemical and ecological variability during the late summer–

early autumn transition at an ice-floe drift station in the Central Arctic Ocean. Limnol. Oceanogr. doi:10.1002/lno.11676

Scharek, R., M. A. Van Leeuwe, and H. J. W. De Baar. 1997. Responses of Southern Ocean phytoplankton to the addition of trace metals. Deep-Sea Res. Part II Top. Stud. Oceanogr. doi:10.1016/S0967-0645(96)00074-4

Schmieder, R., Y. W. Lim, and R. Edwards. 2012. Identification and removal of ribosomal RNA sequences from metatranscriptomes. Bioinformatics **28**: 433–435. doi:10.1093/bioinformatics/btr669

Schneider, B., and J. D. Müller. 2018. Biogeochemical transformations in the Baltic Sea: observations through carbon dioxide glasses, Springer.

Sharp, J. D., D. Pierrot, M. P. Humphreys, J.-M. Epitalon, J. C. Orr, E. R. Lewis, and D. W. R. Wallace. 2023. CO2SYSv3 for MATLAB.doi:10.5281/ZENODO.3950562

Shim, J., D. Kim, Y. C. Kang, J. H. Lee, S.-T. Jang, and C.-H. Kim. 2007. Seasonal variations in pCO2 and its controlling factors in surface seawater of the northern East China Sea. Cont. Shelf Res. **27**: 2623–2636. doi:10.1016/j.csr.2007.07.005

Smith, W. O., A. R. Shields, J. A. Peloquin, G. Catalano, S. Tozzi, M. S. Dinniman, and V. A. Asper. 2006. Interannual variations in nutrients, net community production, and biogeochemical cycles in the Ross Sea. Deep-Sea Res. Part II Top. Stud. Oceanogr. doi:10.1016/j.dsr2.2006.02.014

Sperfeld, E., D. Raubenheimer, and A. Wacker. 2016. Bridging factorial and gradient concepts of resource co-limitation: towards a general framework applied to consumers J. Grover [ed.]. Ecol. Lett. **19**: 201–215. doi:10.1111/ele.12554

Subhas, A. V., J. F. Adkins, S. Dong, N. E. Rollins, and W. M. Berelson. 2019. The carbonic anhydrase activity of sinking and suspended particles in the North Pacific Ocean. Limnol. Oceanogr. **65**: 637–651. doi:10.1002/lno.11332

Sun, Y., P. Debeljak, and I. Obernosterer. 2021. Microbial iron and carbon metabolism as revealed by taxonomy-specific functional diversity in the Southern Ocean. ISME J. **15**: 2933–2946. doi:10.1038/s41396-021-00973-3

Sunda, W. G., and S. A. Huntsman. 1995. Cobalt and zinc interreplacement in marine phytoplankton: Biological and geochemical implications. Limnol. Oceanogr. **40**: 1404–1417. doi:10.4319/lo.1995.40.8.1404

Sunda, W. G., and S. A. Huntsman. 2000. Effect of Zn, Mn, and Fe on Cd accumulation in phytoplankton: Implications for oceanic Cd cycling. Limnol. Oceanogr. **45**: 1501–1516. doi:10.4319/lo.2000.45.7.1501

Sunda, W. G., and S. A. Huntsman. 2005. Effect of CO 2 supply and demand on zinc uptake and growth limitation in a coastal diatom. Limnol. Oceanogr. **50**: 1181–1192. doi:10.4319/lo.2005.50.4.1181

Takahashi, T., S. C. Sutherland, and A. Kozyr. 2020. Global Ocean Surface Water Partial Pressure of CO2 Database (LDEO Database Version 2019): Measurements Performed During 1957-2019 (NCEI Accession 0160492). NOAA Natl. Cent. Environ. Inf.

Tatusov, R. L. and others. 2003. The COG database: an updated version includes eukaryotes. BMC Bioinformatics **4**: 41. doi:10.1186/1471-2105-4-41

Tortell, P. D., M. C. Long, C. D. Payne, A.-C. Alderkamp, P. Dutrieux, and K. R. Arrigo. 2012. Spatial distribution of pCO2, ΔO2/Ar and dimethylsulfide (DMS) in polynya waters and

the sea ice zone of the Amundsen Sea, Antarctica. Deep Sea Res. Part II Top. Stud. Oceanogr. **71–76**: 77–93. doi:10.1016/j.dsr2.2012.03.010

Tortell, P. D., C. Payne, C. Gueguen, R. F. Strzepek, P. W. Boyd, and B. Rost. 2008. Inorganic carbon uptake by Southern Ocean phytoplankton. Limnol. Oceanogr. **53**: 1266–1278. doi:10.4319/lo.2008.53.4.1266

Valerio, A. M., M. Kampel, N. D. Ward, H. O. Sawakuchi, A. C. Cunha, and J. E. Richey. 2021. CO2 partial pressure and fluxes in the Amazon River plume using in situ and remote sensing data. Cont. Shelf Res. **215**: 104348. doi:10.1016/j.csr.2021.104348

Wuttig, K. and others. 2019. Critical evaluation of a seaFAST system for the analysis of trace metals in marine samples. Talanta. doi:10.1016/j.talanta.2019.01.047

Wyatt, N. J., A. Milne, E. M. S. Woodward, A. P. Rees, T. J. Browning, H. A. Bouman, P. J. Worsfold, and M. C. Lohan. 2014. Biogeochemical cycling of dissolved zinc along the GEOTRACES South Atlantic transect GA10 at 40°S. Glob. Biogeochem. Cycles **28**: 44–56. doi:10.1002/2013GB004637

Xu, Y., D. Shi, L. Aristilde, and F. M. M. Morel. 2012. The effect of pH on the uptake of zinc and cadmium in marine phytoplankton: Possible role of weak complexes. Limnol. Oceanogr. doi:10.4319/lo.2012.57.1.0293

Ye, N. and others. 2022. The role of zinc in the adaptive evolution of polar phytoplankton. Nat. Ecol. Evol. **6**: 965–978. doi:10.1038/s41559-022-01750-x

Zhang, Y., Z. Wen, M. P. Washburn, and L. Florens. 2010. Refinements to Label Free Proteome Quantitation: How to Deal with Peptides Shared by Multiple Proteins. Anal. Chem. **82**: 2272–2281. doi:10.1021/ac9023999

**Supplementary information for "Zinc stimulation of phytoplankton in a low carbon dioxide, coastal Antarctic environment: evidence for the Zn hypothesis"**

**Supplementary Table 1. Summary of zinc incubation experiments in marine environments.** Note that all experiments focus on phytoplankton populations with the exception of Fukada et al (2000) and Mazzotta et al. (2021) which focus on bacterial heterotrophy. This list represents our knowledge of the literature but may be incomplete.

| Study | Location | Zn Treatment Replication | $pCO_2$ Data | Dissolved Environmental Zn Data | Zn Response |
|---|---|---|---|---|---|
| Scharek et al. 1997[1] | Southern Ocean | Zn n=2, control n=1 | No | No | Negative/"very small" |
| Fukada et al., 2000[2] | North Pacific | Integrated water column leucine aminopeptidase activity (0-100m) | No | Yes | Leucine aminopeptidase activity positively correlated with dZn |
| Cochlan et al. 2002[3] | Western Ross Sea | None (n=1 +Zn, +Zn+Fe) | No | No | Increase in specific uptake of $NO_3^-$ |
| Coale et al. 2003[4] | Ross Sea, Southern Ocean | None (n=1 +Zn, +Zn+Fe) | No | Yes | Negative/"very small" |
| Crawford et al. 2003[5] | Northeast Pacific Ocean | Triplicate (n=3) | Yes | No | "Slightly but significantly" altered Chl, nitrate and phosphate |
| Franck et al. 2003[6] | Costa Rica Dome | Triplicate (n=3) | No | No | Secondary Zn limitation after Fe in diatom microscopy data |
| Ellwood 2004[7] | Subantarctic | Duplicates (n=2) | No | Yes | Negative |
| Cullen et al. 1999; Cullen and Sherrell 2005[8,9] | Coastal California | Duplicates (n=2) | No | No | Enhanced Cd:P in low $pCO_2$ treatments, decrease in Cd:P with Zn addition |
| Jakuba et al. 2012[10] | North Pacific | Singlicate with timepoints sacrificed | No | Yes | Primary, no additive effect with iron. |
| Dreux Chappell et al. 2016[11] | Costa Rica Dome | Triplicate (n=3) | No | Yes | Secondary limitation with Si |
| Sharma et al. 2020[12] | Eastern Arabian Sea | Triplicate (n=3) | Yes | No | Negative/ "insignificant effects" |
| Mazzotta et al. 2021[13] | Equatorial Pacific | Quintuplicate (n=5) sediment trap incubations | No | Yes in separate study (Cohen et al., 2021) | Enhancement of alkaline phosphatase activity with Zn addition in sediment trap samples |
| This study | Terra Nova Bay, Ross Sea | Triplicate (n=3) | Yes | Yes | Primary and Secondary limitation. Independent validation by Zn biomarkers. |

**Supplementary Table 2**. Station metadata for the NBP18-01 cruise. Stations at which total Zn uptake rates were determined are indicated by asterisks (*).

| Station | Latitude (°N) | Longitude (°E) | Sampling Date (yyyy-mm-dd hh:mm) |
|---|---|---|---|
| 4* | -72.751 | -116.001 | 2017-12-30 01:23 |
| 10 | -73.054 | -129.988 | 2018-01-03 03:39 |
| 11* | -74.047 | -133.764 | 2018-01-03 19:58 |
| 15* | -75.864 | -151.918 | 2018-01-05 14:51 |
| 20* | -76.714 | 179.819 | 2018-01-08 02:00 |
| 22* | -75.013 | 165.358 | 2018-01-09 15:56 |
| 25 | -75.293 | 163.914 | 2018-01-11 01:26 |
| 27* | -74.987 | 165.890 | 2018-01-11 16:05 |
| 29* | -76.001 | 172.997 | 2018-01-16 03:00 |
| 31 | -77.295 | 175.390 | 2018-01-17 04:39 |
| 32* | -76.750 | 172.000 | 2018-01-17 19:19 |
| 34 | -77.147 | 168.503 | 2018-01-23 22:59 |
| 35* | -76.231 | 168.769 | 2018-01-26 20:17 |
| 41* | -74.833 | 165.002 | 2018-01-29 00:41 |
| 46* | -74.742 | 165.287 | 2018-01-31 21:32 |
| 50 | -74.741 | 165.488 | 2018-02-02 21:17 |
| 52* | -75.000 | 164.005 | 2018-02-03 21:43 |
| 57* | -74.879 | 164.482 | 2018-02-06 20:12 |
| 60 | -74.959 | 164.739 | 2018-02-08 20:06 |
| 62* | -74.999 | 169.491 | 2018-02-09 19:27 |
| 67* | -76.454 | 167.919 | 2018-02-11 19:19 |
| 70 | -74.744 | 170.374 | 2018-02-13 21:25 |
| 72* | -74.800 | 164.395 | 2018-02-14 22:28 |
| 76* | -74.799 | 164.597 | 2018-02-16 20:15 |
| 78 | -74.696 | 164.796 | 2018-02-17 20:34 |
| 79* | -74.757 | 164.356 | 2018-02-18 19:29 |

**Supplementary Table 3**. Summary of ANOVA statistics for T6 incubation treatments comparing measured parameters. Significant differences among groups were found using one-way ANOVA and post-hoc Dunnett test (*** p < 0.001, ** p < 0.01, * p < 0.05, . p < 0.1). Chl *a,* chlorophyll *a;* $DIC_T$, total dissolved inorganic carbon; chl *b,* chlorophyll *b*; Prasino, prasinoxanthin; fuco, fucoxanthin; 19'hex, 19'-hexanoyloxyfucoxanthin; chl c3, chlorophyll c3. NA, no statistically significant difference. All parameters were measured in biological triplicate.

| Treatment (T6) | Chl *a* | $DIC_T$ | Chl *b* | Prasino | Fuco | 19'hex | Fuco:hex | Hex:Chl c3 | Bacterial abundance |
|---|---|---|---|---|---|---|---|---|---|
| +Fe vs Ctrl | *p* = 9.5e-5 (***) | *p* = 5.3e-6 (***) | *p* = 4.0e-3 (**) | *p* = 2.9e-2 (*) | NA | *p* = 8e-3 (**) | *p* = 4.2e-4 (***) | *p* = 2.0e-4 (***) | *p* = 9.1e-4 (***) |
| +Zn vs Ctrl | *p* = 1.1e-2 (*) | *p* = 5.0e-6 (***) | *p* = 8.0e-2 (.) | *p* = 7.4e-3 (**) | NA | NA | NA | *p* = 0.02520 (*) | NA |
| +FeZn vs Ctrl | *p* = 1.3e-7 (***) | *p* = 2.2e-16 (***) | *p* = 4.0e-4 (***) | *p* = 5.7e-2 (.) | NA | NA | *p* = 2.7e-3 (**) | *p* = 1.9e-4 (***) | *p* = 6.3e-4 (***) |
| +FeZn vs +Fe | *p* = 3.4e-2 (*) | *p* = 4.4e-3 (**) | NA | NA | NA | *p* = 6.0e-2 (.) | NA | NA | NA |

**Supplementary Table 4.** Representative proteins of interest, reference organism and IDs.

| Protein of interest | Reference organism | Protein ID |
|---|---|---|
| ZCRP-A | *Thalassiosira pseudonana* CCMP1335 | 3054 (JGI Thaps3[*]) |
| ZCRP-B | *Thalassiosira pseudonana* CCMP1335 | 938 (JGI Thaps3_bd[**]) |
| RUBISCO | *Phaeodactylum tricornutum* CCMP632 | AAF07200.1 (NCBI) |
| ISIP1A | *Thalassiosira oceanica* CCMP1005 | K0RCT3 (Uniprot) |
| ISIP2A | *Phaeodactylum tricornutum* CCMP632 | B7FYL2 (Uniprot) |
| ISIP3 | *Phaeodactylum tricornutum* CCMP632 | B7G4H8 (Uniprot) |
| ZIP | *Phaeodactylum tricornutum* CCMP632 | 46780 (JGI Phatr2[†]) |
| CDCA | *Thalassiosira pseudonana* CCMP1335 | 25840 (JGI Thaps3[*]) |

[*]Joint Genome Institute (JGI) Thaps3 database (https://mycocosm.jgi.doe.gov/Thaps3/Thaps3.home.html)

[**]Joint Genome Institute Thaps3_bd database (https://mycocosm.jgi.doe.gov/Thaps3_bd/Thaps3_bd.home.html

[†]Joint Genome Institute CCAP 1055/1 v2.0 Phatr2, all models database (https://mycocosm.jgi.doe.gov/Phatr2/Phatr2.home.html)

**Supplementary Table 5**. Particulate Zn:P ratios measured in *T. pseudonana* cultured at various concentrations of Zn (log [Zn′]) (Sunda and Huntsman 2005) compared to particulate Zn:P ratios measured at Station 27 of research cruise NBP18-01. Zn:C measurements by Sunda and Huntsman 2005 were converted to Zn:P using the Redfield ratio. Data is plotted in Supplementary Figure 6. Zn′ refers to the sum of inorganic Zn metal complexes.
+Particulate P data measured directly in this study
*Particulate P from Sunda 2005 data was estimated by converting particulate C measurements to P using the Redfield ratio (106C:1P).

| **Particulate Zn:P ratios at Station 27** | | | | | | | |
|---|---|---|---|---|---|---|---|
| Depth (m) | | | Particulate Zn (mol) | | Particulate P (mol)+ | Zn:P (mol:mol) | |
| 100 | | | 1E-11 | | 8E-08 | 1E-04 | |
| 50 | | | 1E-11 | | 1E-07 | 1E-04 | |
| 25 | | | 3E-11 | | 2E-07 | 2E-04 | |
| 10 | | | 4E-11 | | 2E-07 | 2E-04 | |
| **Cellular Zn:P ratios of cultured *T. pseudonana* from Sunda and Huntsman 2005, Table 1.** | | | | | | | |
| Experiment | Log [Zn'] | pH | Particulate Zn (mol) | Particulate C (mol) | Particulate P (mol)* | Zn:P (mol:mol) | Growth rate ($d^{-1}$) |
| 1 | -12.05 | 8.2 | 3.3E-05 | 22 | 0.21 | **2E-04** | **0.1** |
| 1 | -11.47 | 8.2 | 5.2E-05 | 15 | 0.14 | 4E-04 | 1.23 |
| 1 | -10.87 | 8.2 | 1.2E-04 | 15 | 0.14 | 9E-04 | 1.62 |
| 1 | -10.36 | 8.2 | 1.5E-04 | 15 | 0.14 | 1E-03 | 1.76 |
| 1 | -9.82 | 8.2 | 1.8E-04 | 15 | 0.14 | 1E-03 | 1.76 |
| 1 | -11.96 | 9 | 3.8E-05 | 15 | 0.14 | 3E-04 | 0.51 |
| 1 | -11.38 | 9 | 8.5E-05 | 15 | 0.14 | 6E-04 | 1.12 |
| 1 | -10.78 | 9 | 2.0E-04 | 15 | 0.14 | 1E-03 | 1.28 |
| 1 | -10.27 | 9 | 4.1E-04 | 15 | 0.14 | 3E-03 | 1.42 |
| 1 | -9.73 | 9 | 5.0E-04 | 15 | 0.14 | 4E-03 | 1.49 |
| 2 | -11.82 | 8.2 | 4.9E-05 | 15 | 0.14 | 3E-04 | 0.64 |
| 2 | -11.82 | 8.2 | 4.0E-05 | 15 | 0.14 | 3E-04 | 0.79 |
| 2 | -10.87 | 8.2 | 1.3E-04 | 15 | 0.14 | 9E-04 | 1.45 |
| 2 | -9.82 | 8.2 | 2.0E-04 | 15 | 0.14 | 1E-03 | 1.51 |
| 2 | -11.71 | 9 | 5.8E-05 | 15 | 0.14 | 4E-04 | 0.73 |
| 2 | -11.71 | 9 | 5.8E-05 | 15 | 0.14 | 4E-04 | 0.78 |
| 2 | -10.76 | 9 | 1.9E-04 | 15 | 0.14 | 1E-03 | 1.39 |
| 2 | -10.76 | 9 | 2.1E-04 | 15 | 0.14 | 1E-03 | 1.38 |
| 2 | -9.71 | 9 | 4.3E-04 | 15 | 0.14 | 3E-03 | 1.44 |
| 2 | -9.71 | 9 | 5.0E-04 | 15 | 0.14 | 4E-03 | 1.42 |
| 4 | -11.82 | 8.2 | 2.8E-05 | 18.1 | 0.21 | 3E-04 | 0.72 |
| 4 | -11.32 | 8.2 | 5.5E-05 | 15.2 | 0.13 | 4E-04 | 1.45 |
| 4 | -10.82 | 8.2 | 1.3E-04 | 14.7 | 0.14 | 9E-04 | 2 |
| 4 | -10.32 | 8.2 | 2.2E-04 | 15.1 | 0.14 | 2E-03 | 2.03 |
| 4 | -9.82 | 8.2 | 2.6E-04 | 15.6 | 0.14 | 2E-03 | 2.04 |

**Supplementary Table 6**. Reference seawater comparisons using the 2009 GEOTRACES coastal surface seawater (GSC) standard.

| Metal | This study (n = 8) (nM) | GEOTRACES GSC consensus (nM) |
|---|---|---|
| Fe | 1.6 ± 0.23 | 1.6 ± 0.12 |
| Zn | 1.4 ± 0.23 | 1.5 ± 0.10 |
| Cd | 0.4 ± 0.01 | 0.4 ± 0.02 |
| Cu | 1.3 ± 0.05 | 1.1 ± 0.15 |
| Ni | 4.2 ± 0.07 | 4.5 ± 0.21 |
| Mn | 2.1 ± 0.37 | 2.2 ± 0.08 |

## Supplementary Figures

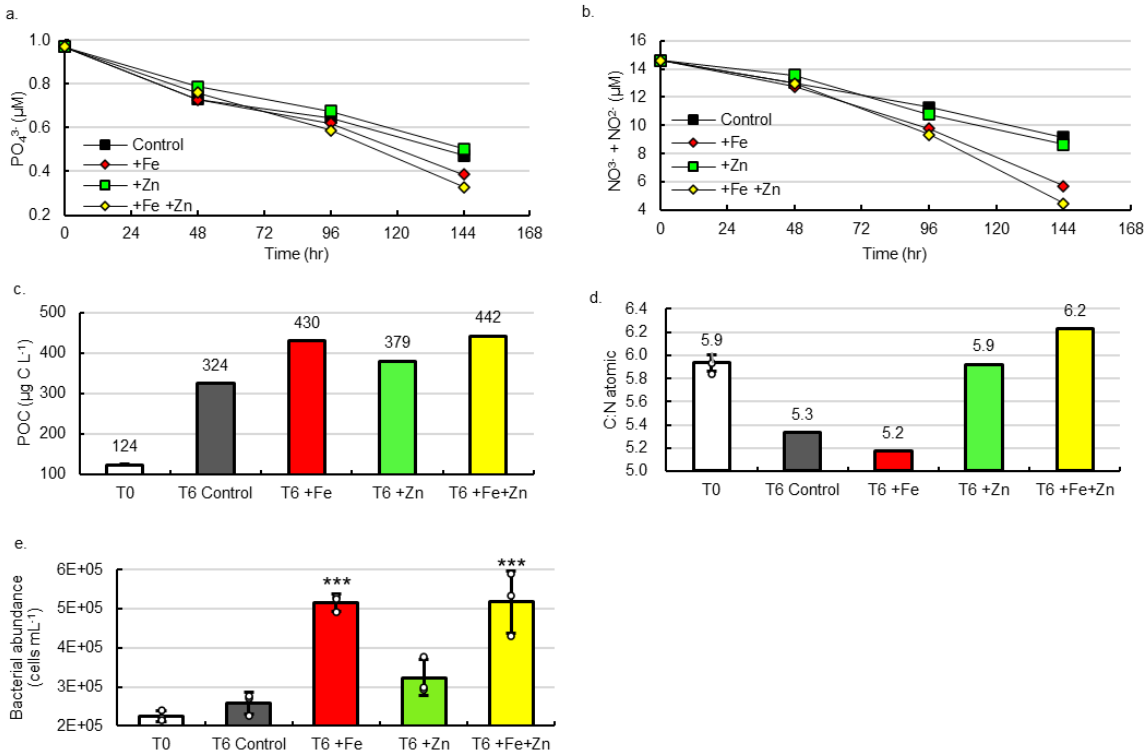


**Supplementary Figure 1. Additional parameters measured in shipboard bottle incubations**. Time course decreases in (**a**) phosphate and (**b**) nitrite + nitrate. (**c**) total POC of biomass in each treatment at T6. (**d**) the atomic carbon:nitrogen (C:N) ratio of biomass in each treatment at T6, and (**e**) bacterial abundance. Significant differences among groups were found using one-way ANOVA and post-hoc Dunnett test (*** $p < 0.001$, ** $p < 0.01$, * $p < 0.05$). Error bars are the standard deviation of biological triplicates (n=3) with individual data points overlaid (white

circles). Macronutrients, POC, and PON were measured in singlicate (n=1) from pooled biological triplicates.

a.

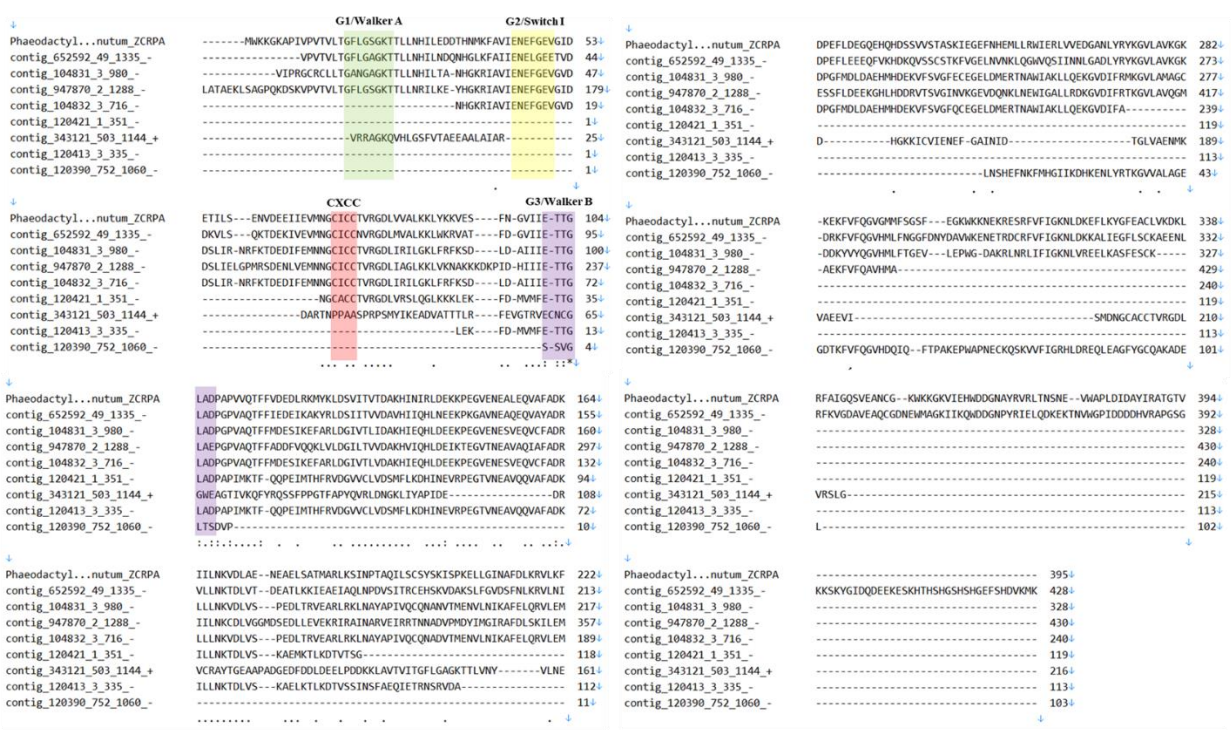


b.

| orf_id | Hit | E value | % ID |
|---|---|---|---|
| contig_652592_49_1335_- | Phaeodactylum_tricornutum_ZCRPA | 4.75E-162 | 56.266 |
| contig_104831_3_980_- | Phaeodactylum_tricornutum_ZCRPA | 6.51E-110 | 50.311 |
| contig_947870_2_1288_- | Phaeodactylum_tricornutum_ZCRPA | 5.00E-86 | 49.488 |
| contig_104832_3_716_- | Phaeodactylum_tricornutum_ZCRPA | 5.25E-80 | 48.954 |
| contig_120421_1_351_- | Phaeodactylum_tricornutum_ZCRPA | 1.62E-32 | 51.818 |
| contig_343121_503_1144_+ | Phaeodactylum_tricornutum_ZCRPA | 3.24E-23 | 60.526 |
| contig_120413_3_335_- | Phaeodactylum_tricornutum_ZCRPA | 5.54E-22 | 41.964 |
| contig_120390_752_1060_- | Phaeodactylum_tricornutum_ZCRPA | 7.76E-13 | 41.111 |

**Supplementary Figure 2. Sequence alignments of ZCRP-A peptides detected in T6 incubation biomass. (a)** Sequence alignment of the *Phaeodactylum tricornutum* ZCRP-A protein compared to all ZCRP-A proteins detected in T6 incubation biomass. Alignment was generated using the MUSCLE algorithm with default parameters within MEGA11. Four conserved GTPase (G1/Walker A, G2/SwitchI, CXCC metal binding, and G3/Walker B) are labeled. (**b**) E values and % identities of the identified proteins with significant sequence similarity to *P. tricornutum* ZCRP-A aligned above.

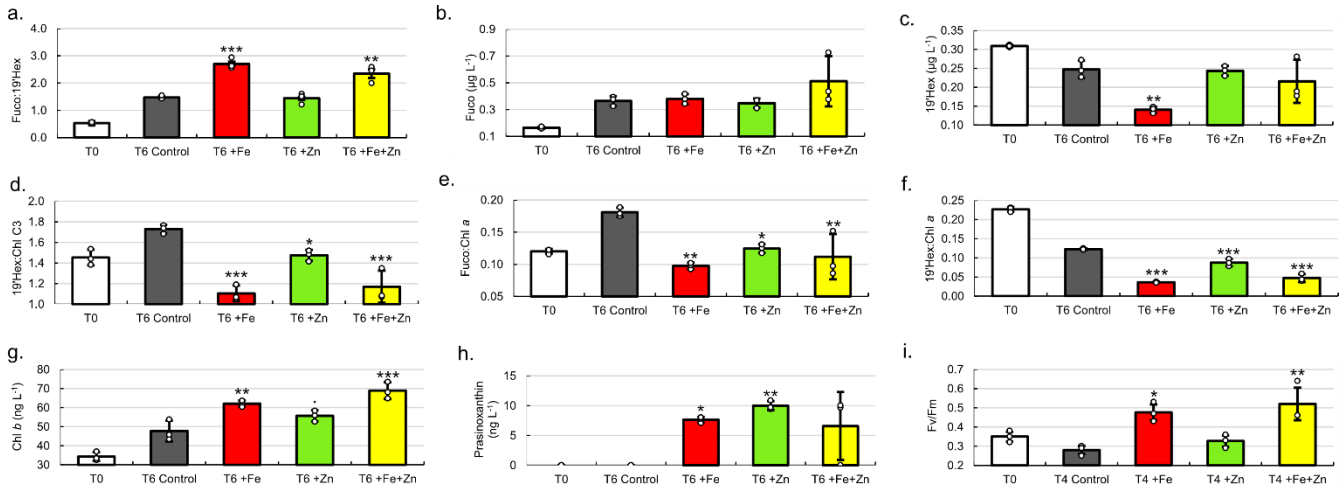


**Supplementary Figure 3. Pigment analysis of T6 incubations**. (**a**) ratio of fucoxanthin: 19'-Hex, (**b**) fucoxanthin, (**c**) 19-hexanoyloxyfucoxanthin (19'-Hex), (**d**) ratio of 19'-Hex: chl c3, (**e**) ratio of fucoxanthin: chlorophyll *a*, (**f**) ratio of 19'-Hex: chlorophyll *a*, (**g**) chlorophyll *b*, (**h**) prasinoxanthin, and (**i**) maximum quantum efficiency (Fv/Fm) among treatments at T4. Significant differences among groups were found using one-way ANOVA and post-hoc Dunnett test (*** $p < 0.001$, ** $p < 0.01$, * $p < 0.05$, . $p < 0.1$). Data with error bars are presented as mean values ± the standard deviation of biological triplicates (n=3) with individual data points overlaid (white circles).

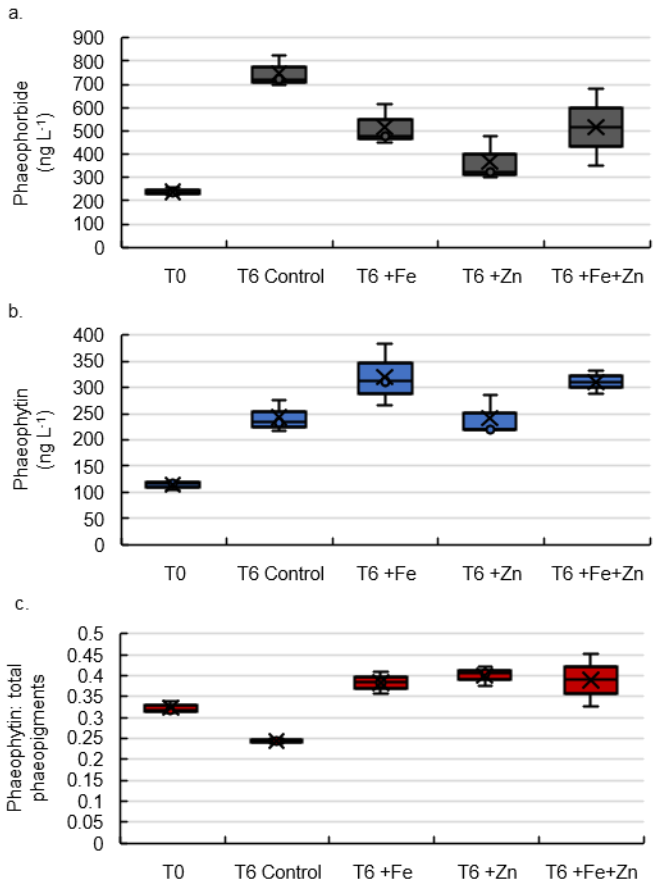


**Supplementary Figure 4.** Phaeopigments measured in T6 incubation biomass. Abundances of (**a**) phaeophorbide and (**b**) phaeophytin, and (**c**) the ratio of phaeophytin: total phaeopigments (the sum of phaeophorbide and phaeophytin). Error bars are the standard deviation of biological triplicates (n=3).

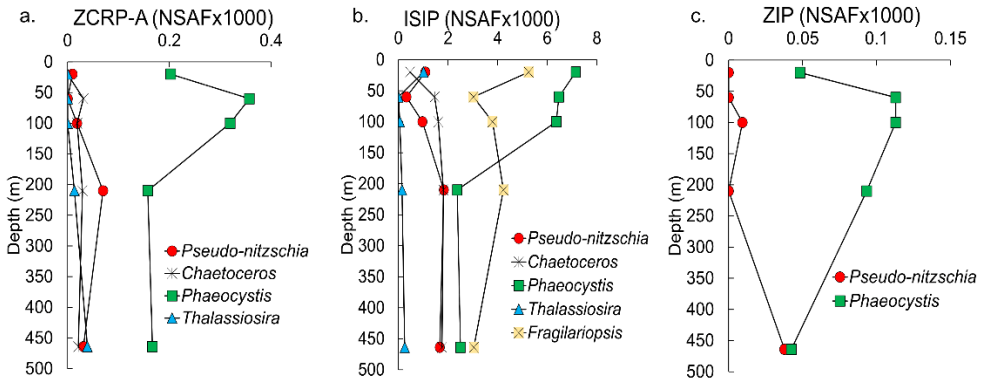


**Supplementary Figure 5. Depth profiles for proteins of interest at station 27 categorized by genus.** Depth profiles of NSAF-normalized protein spectral counts of (**a**) ZCRP-A, (**b**), iron starvation induced proteins (ISIPs), and (**c**) ZIPs summed by genus. Proteins assigned to an individual genus were summed across all size fractions (0.2, 3 and 51 μm). ISIPs are the combined spectral counts of ISIP1A, ISIP2A and ISIP3.

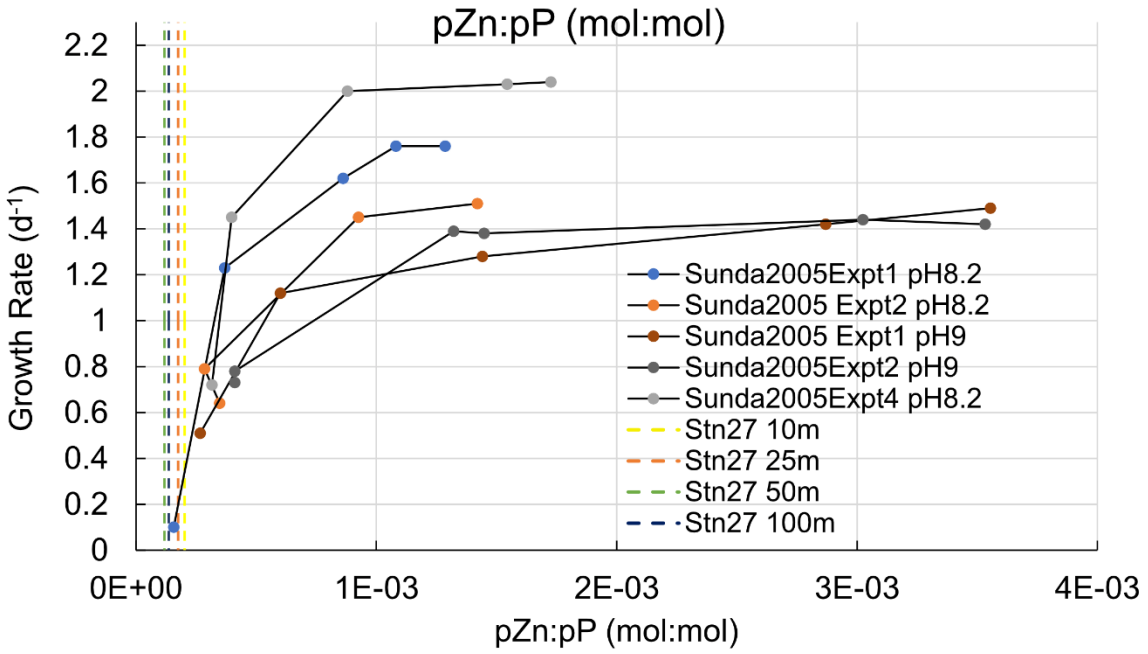


**Supplementary Figure 6. Comparison of particulate Zn: particulate P ratios measured in the water column at the experimental site to those ratios measured in culture studies of a Zn-limited diatom.** Ratio of particulate Zn (pZn) and particulate phosphorus (pP) (pZn:pP) measured in the upper water column at the study site (station 27; vertical dashed lines) compared to pZn:pP measurements in Zn limitation studies of the diatom *Thalassiosira pseudonana* in culture by Sunda and Huntsman 2005.

**Supplementary Information References**


1. Scharek, R., Van Leeuwe, M. A. & De Baar, H. J. W. Responses of Southern Ocean phytoplankton to the addition of trace metals. *Deep-Sea Res. Part II Top. Stud. Oceanogr.* (1997) doi:10.1016/S0967-0645(96)00074-4.
2. Fukuda, R. *et al.* East—west gradient in ectoenzyme activities in the subarctic Pacific: Possible regulation by zinc. *Limnol. Oceanogr.* **45**, 930–939 (2000).
3. Cochlan, W. P., Bronk, D. A. & Coale, K. H. Trace metals and nitrogenous nutrition of Antarctic phytoplankton: experimental observations in the Ross Sea. *Deep Sea Res. Part II Top. Stud. Oceanogr.* **49**, 3365–3390 (2002).
4. Coale, K. H., Wang, X., Tanner, S. J. & Johnson, K. S. Phytoplankton growth and biological response to iron and zinc addition in the Ross Sea and Antarctic Circumpolar Current along 170°W. *Deep Sea Res. Part II Top. Stud. Oceanogr.* **50**, 635–653 (2003).
5. Crawford, D. W. *et al. Influence of Zinc and Iron Enrichments on Phytoplankton Growth in the Northeastern Subarctic Pacific Limitation of Biomass and Primary Production of Phyto-Plankton by Dissolved Iron (Fe) in High-Nutrient, Low-Chlo*. *Limnol. Oceanogr* vol. 48 1583–1600 (2003).
6. Franck, V., Bruland, K., Hutchins, D. & Brzezinski, M. Iron and zinc effects on silicic acid and nitrate uptake kinetics in three high-nutrient, low-chlorophyll (HNLC) regions. *Mar. Ecol. Prog. Ser.* **252**, 15–33 (2003).
7. Ellwood, M. J. Zinc and cadmium speciation in subantarctic waters east of New Zealand. *Mar. Chem.* (2004) doi:10.1016/j.marchem.2004.01.005.

8. Cullen, J. T., Lane, T. W., Morel, F. M. M. & Sheerell, R. M. Modulation of cadmium uptake in phytoplankton by seawater CO2 concentration. *Nature* (1999) doi:10.1038/46007.

9. Cullen, J. T. & Sherrell, R. M. Effects of dissolved carbon dioxide, zinc, and manganese on the cadmium to phosphorus ratio in natural phytoplankton assemblages. *Limnol. Oceanogr.* **50**, 1193–1204 (2005).

10. Jakuba, R. W., Saito, M. A., Moffett, J. W. & Xu, Y. Dissolved zinc in the subarctic North Pacific and Bering Sea: Its distribution, speciation, and importance to primary producers. *Glob. Biogeochem. Cycles* (2012) doi:10.1029/2010GB004004.

11. Dreux Chappell, P. *et al.* Preferential depletion of zinc within Costa Rica upwelling dome creates conditions for zinc co-limitation of primary production. *J. Plankton Res.* **38**, 244–255 (2016).

12. Sharma, D. *et al.* Impacts of Zn and Cu enrichment under ocean acidification scenario on a phytoplankton community from tropical upwelling system. *Mar. Environ. Res.* **155**, 104880 (2020).

13. Mazzotta, M. G. *et al.* Characterization of the metalloproteome of Pseudoalteromonas (BB2-AT2): biogeochemical underpinnings for zinc, manganese, cobalt, and nickel cycling in a ubiquitous marine heterotroph. *Metallomics* **13**, (2021).

14. Sunda, W. G. & Huntsman, S. A. Effect of CO2 supply and demand on zinc uptake and growth limitation in a coastal diatom. *Limnol. Oceanogr.* **50**, 1181–1192 (2005).

15. Lauvset, S. K. *et al.* GLODAPv2.2022: the latest version of the global interior ocean biogeochemical data product. *Earth Syst. Sci. Data* **14**, 5543–5572 (2022).

16. Jiang, L. *et al.* Global Surface Ocean Acidification Indicators From 1750 to 2100. *J. Adv. Model. Earth Syst.* **15**, e2022MS003563 (2023).